Langmuir

ARTICLE

pubs.acs.org/Langmuir

Saccharide-Functionalized Alkanethiols for Fouling-Resistant Self-Assembled Monolayers: Synthesis, Monolayer Properties, and Antifouling Behavior

Timmy Fyrner,[†] Hung-Hsun Lee,[‡] Alberto Mangone,[‡] Tobias Ekblad,[‡] Michala E. Pettitt,[§] Maureen E. Callow,[§] James A. Callow,[§] Sheelagh L. Conlan,[∥] Robert Mutton,[∥] Anthony S. Clare,[∥] Peter Konradsson,[†] Bo Liedberg,[‡] and Thomas Ederth*[,‡]

[†]Division of Chemistry and [‡]Division of Molecular Physics, IFM, Linköping University, SE-581 83 Linköping, Sweden

[§]School of Biosciences, University of Birmingham, Birmingham B15 2TT, United Kingdom

[∥]School of Marine Science and Technology, Newcastle University, Newcastle upon Tyne NE1 7RU, United Kingdom

Supporting Information

ABSTRACT: We describe the synthesis of a series of mono-, di-, and trisaccharide-functionalized alkanethiols as well as the formation of fouling-resistant self-assembled monolayers (SAMs) from these. The SAMs were characterized using ellipsometry, wetting measurements, and infrared reflection−absorption spectroscopy (IRAS). We show that the structure of the carbohydrate moiety affects the packing density and that this also alters the alkane chain organization. Upon increasing the size of the sugar moieties (from mono- to di- and trisaccharides), the structural qualities of the monolayers deteriorated with increasing disorder, and for the trisaccharide, slow reorganization dynamics in response to changes in the environmental polarity were observed. The antifouling properties of these SAMs were investigated through protein adsorption experiments from buffer solutions as well as settlement (attachment) tests using two common marine fouling species, zoospores of the green macroalga *Ulva linza* and cypris larvae of the barnacle *Balanus amphitrite*. The SAMs showed overall good resistance to fouling by both the proteins and the tested marine organisms. To improve the packing density of the SAMs with bulky headgroups, we employed mixed SAMs where the saccharide−thiols are diluted with a filler molecule having a small 2-hydroxyethyl headgroup. This method also provides a means by which the steric availability of sugar moieties can be varied, which is of interest for specific interaction studies with surface-bound sugars. The results of the surface dilution study and the low nonspecific adsorption onto the SAMs both indicate the feasibility of this approach.

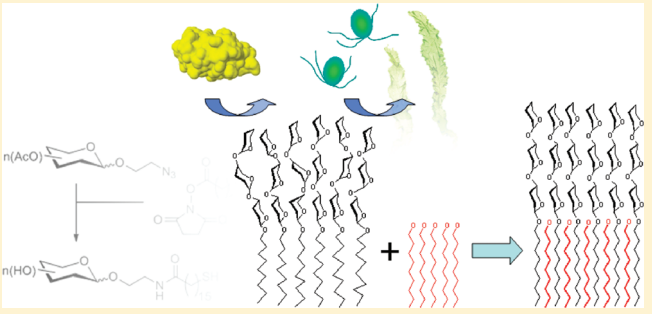

INTRODUCTION

Sugars play diverse and complex roles in the chemistry of nature, for example, in immune response and cell recognition, as cell-protecting physical barriers, and as modulators of protein−protein interactions. The detailed determination of glycoconjugate structures remains a challenge because the precise structure of glycans is not genetically coded, and the combinatorial possibilities in the linkage of two monosaccharides exceeds by far those of, for example, two amino acids or two nucleic acids, resulting in considerable structural variety. For a long time, studies of the structure/function relationship of saccharides lagged behind those of other (biological) macromolecules because of their complexity and the lack of suitable characterization methods. However, as such methods have been successively developed, progress in the area has been rapid, and the biology of saccharides is now both a large and quickly growing area of research, with applications in biotechnology, pharmaceuticals, and biomedicine.[1] This also implies that effective means required to exploit the properties of sugars are available, and by taking advantage of the diversity and flexibility offered via carbohydrate synthesis, many new possibilities have emerged in materials science[2,3] and in particular biomaterials[4,5] for bioanalytical applications,[6,7] such as the production of well-defined surfaces with interesting antifouling properties using polysaccharides,[8−10] oligosaccharide-terminated SAMs,[11−13] or polyols.[14−16]

The use of SAMs for studies of protein−surface interactions is widespread in antifouling research. As a result of extensive research, SAMs exposing oligoethylene glycols[11,17−19] are well known for their protein-resistant properties. In previous studies,[12,13] it was observed that galactose-terminated alkanethiols can be used to form well-defined, protein-resistant SAMs that also perform well in laboratory marine biofouling assays. This is of interest for several

Received: July 19, 2011
Revised: November 1, 2011
Published: November 04, 2011

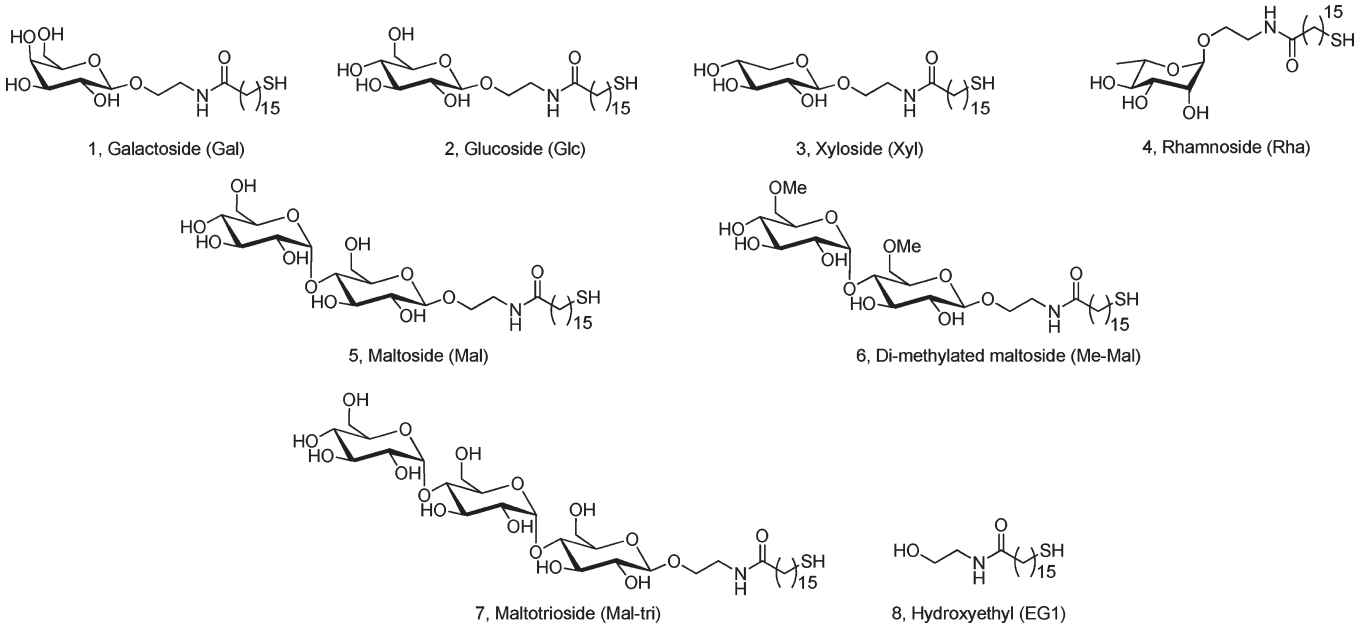

Figure 1. Synthesized carbohydrate- and hydroxyethyl-terminated alkanethiols for interaction studies using model proteins and marine fouling species.

Scheme 1. General Preparation of Glycosyl-Terminated Alkanethiols 2−5 and 7[a]

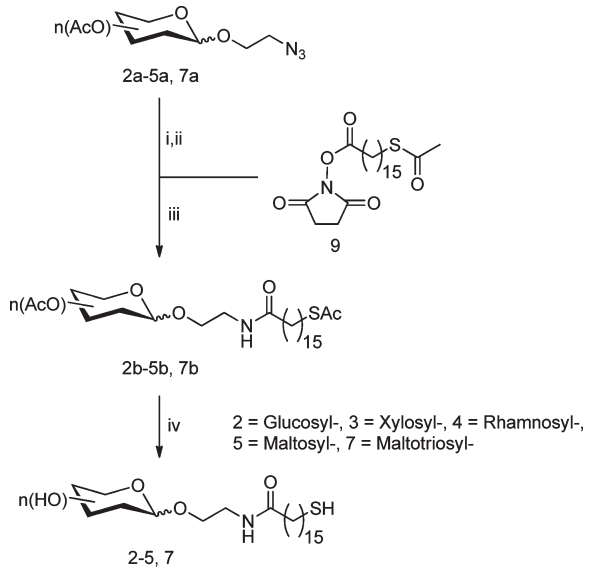

[a] (i) Boc_2O, EtOH, 10% Pd/C. (ii) TFA/CH_2Cl_2. (iii) **9**, DIPEA, DMF, 61−77%. (iv) K_2CO_3, MeOH, 73−97%.

reasons: the hydroxyl-rich SAMs show very good inhibition of protein adsorption, which is reasonably consistent with previous studies of sugar-terminated SAMs[11,14] but inconsistent with earlier work suggesting that protein-resistant surfaces must not contain hydrogen bond donors.[20] In a marine biofouling study,[13] we compared monosaccharide-terminated SAMs with mixed monolayers of methyl- and hydroxyl-terminated alkanethiols, demonstrating that the interactions of marine organisms with surfaces having similar wettabilities and exposing similar functional groups varied depending on differences in the molecular structure and, in particular, the resulting differences in the structure of interfacial water. Because of the steric constraints in accessibility of the sugars in the monolayer, it is unlikely that the observed differences result from specific interactions with sugar groups on the surface. Because cell attachment to surfaces is frequently mediated by cell-surface-bound lectins specifically interacting with sugars on the substrate, this could be an interesting route to investigate by increasing the steric availability of sugar moieties on the surface. There are also a number of examples of how specific interactions with sugars affect the behavior of marine fouling organisms. (See, for example, section 6.4 of Railkin.[21])

To continue our previous studies,[13] we set out to investigate the importance of the molecular structure of various monosaccharides and the effects of the size of the saccharide moieties using di- and trisaccharides. Both interactions with model proteins and with the settling (attaching) stages of two marine fouling species are studied. Thus, herein we describe the synthesis of five carbohydrate-based (glucosyl-, rhamnosyl-, xylosyl-, maltosyl-, and maltotriosyl-) alkanethiols (**2**−**5**,**7**, Figure 1) in a four-step manner, starting from the corresponding, easily available 2-azidoglycosides. Also, the synthesis of a 6,6′-dimethylated maltosyl derivative is described (**6**, Figure 1). Derivative **1** was synthesized according to published procedures.[12] In all derivatives, an amide-linked ω-functionalized hexadecane alkanethiol group has been employed; long alkane chains are frequently used to increase the order and stability in SAMs. The presented functionalized alkanethiols were used to form SAMs on gold surfaces, and the structures of these SAMs were characterized using ellipsometry, contact angle goniometry, tensiometry, and IRAS. As a means to improve the order and density of the monolayers, we also investigate how mixing the saccharides with a hydroxyethyl-terminated filler molecule **8**, with a much smaller headgroup, affects the structure of the layers. The filler molecule was synthesized according to published methods.[22] Surface dilution of the saccharides is also an approach to exposing the saccharide moieties, permitting access to proteins, and making possible studies of specific interaction with the sugar moieties.[23,24] To assess the resistance of these SAMs to protein fouling, we have

dx.doi.org/10.1021/la202774e |*Langmuir* 2011, 27, 15034–15047

performed experiments where model proteins (bovine serum albumin (BSA), lysozyme, fibrinogen, and pepsin) were adsorbed from buffer solutions. Furthermore, initial experiments using the settling (attaching) stages of two common marine fouling organisms were performed, viz., zoospores of a green macroalga (*Ulva linza*) and cypris larvae of a barnacle (*Balanus amphitrite*), indicating areas of future interest for studies using these coatings.

RESULTS AND DISCUSSION

Thiol Synthesis. Alkanethiols **2**−**5** and **7** were all synthesized according to the route outlined in Scheme 1.

Starting from the known 2-azidoethyl glycosides[25−27] (**2a**−**5a**), conversion of the azides to the corresponding amines was performed in a two-step sequence starting with hydrogenation using 10% Pd/C in absolute ethanol with Boc_2O present, followed by deprotection of the Boc group using TFA in CH_2Cl_2. Having Boc_2O present during the reduction of the azido group hinders the migration of the acyl group. The amine was subsequently acylated using *N*-hydroxysuccinimide ester **9**[28] and DIPEA in DMF achieving saccharide-terminated derivatives **2b**−**5b** and **7b** in 61−77% yield over three steps. *Per*-acetylated compounds **2b**−**5b** and **7b** could all be deprotected under mild basic conditions using K_2CO_3 in MeOH to give target molecules **2**−**5** and **7** in 73−97% yields. 2-Azidoethyl glycoside **7a** was synthesized from maltotriose and 2-azidoethanol,[25] using $BF_3 \cdot OEt_2$ as a promotor, in 44% yield (Scheme 2).

In the synthesis of target molecule **6**, glycoside **5a** was first deprotected under Zemplén conditions, followed by selective protection of the two primary hydroxyl groups using TBDPSCl, imidazole, and DMAP in DMF. The remaining hydroxyls were benzylated with BnBr and with NaH in DMF to give the desired compound **11** in 83% yield over two steps. Deprotection of the silyl ethers using TBAF in THF followed by methylation using MeI and NaH in DMF gave the desired 6,6′-*O*-dimethylated derivative **12** in 86% yield over two steps. Hydrogenation, using 20% $Pd(OH)_2/C$ in EtOH/HOAc (9:1), removed the benzyl groups and unmasked the amine that was subsequently acylated using *N*-hydroxysuccinimide ester **9** and DIPEA in DMF to achieve compound **13** in 65% yield. The thioacetyl group was finally readily deprotected under mild basic conditions using K_2CO_3 in MeOH, resulting in final thiol **6** in an overall yield of 39% from 2-azidoglycoside (**5a**).

Contact Angle and Ellipsometry Measurements. The wettability of a surface reflects properties at the outermost few atomic layers. All prepared SAMs, except the one containing derivative **6**, showed very hydrophilic behavior with nearly complete wetting (Table 1). The SAM produced from **6** has a less hydrophilic surface with advancing and receding contact angles of 44 and 21°, respectively. This hysteresis indicates a certain degree of surface inhomogeneity, which is attributed to conformational freedom due to a low degree of molecular packing, as also confirmed by IRAS spectra. To discriminate the saccharides' wettabilities, the

Scheme 2. (i) (a) Ac_2O, NaOAc, Toluene, Reflux; (b) 2-Azidoethanol, $BF_3 \cdot OEt_2$, 4 Å MS, CH_2Cl_2

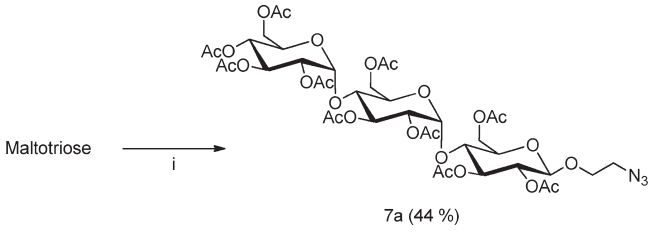

Scheme 3. (i) NaOMe, MeOH; (ii) TBDPSCl, Imidazole, DMAP, DMF; (iii) BnBr, NaH, DMF, 83%; (iv) TBAF, THF; (v) MeI, NaH, DMF, 86%; (vi) 20% $Pd(OH)_2/C$, EtOH/HOAc (9:1); (vii) 9, DIPEA, DMF, 65%; (viii) K_2CO_3, MeOH, 83%

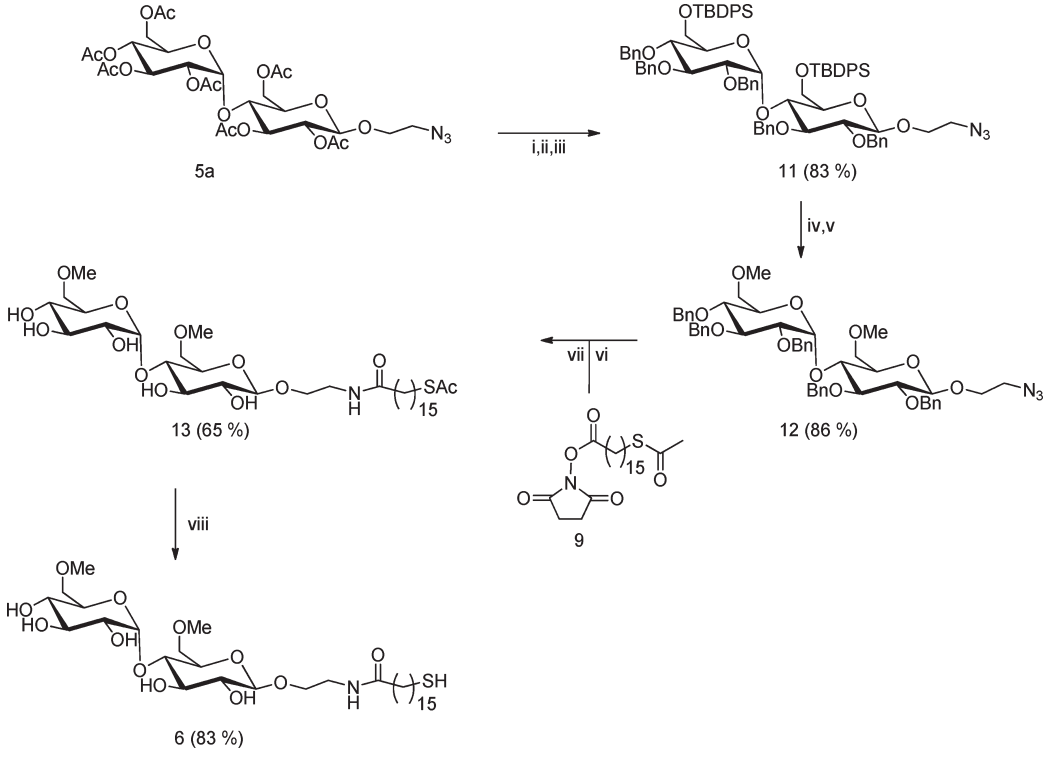

dx.doi.org/10.1021/la202774e |*Langmuir* 2011, 27, 15034–15047

Table 1. Ellipsometric Thickness *d*, Advancing (θ_a) and Receding (θ_r) Contact angles, Amide II Peak Positions, and Integrated Areas of the Amide II Band (Relative to That of 8), of the Single-Component Saccharide-Terminated Alkanethiol SAMs on Gold

	ellipsometric thickness	contact angles by goniometry (deg)		contact angles by tensiometry (deg)			
sample	d (Å)	$\theta_a \pm 1$	$\theta_r \pm 1$	$\theta_a \pm 1$	$\theta_r \pm 2$	amide II peak position (cm^{-1})	relative amide II area
1, galactoside	27.7 ± 0.2	<10		6	4	1553	0.57
2, glucoside	27.9 ± 0.2	<10		0	0	1553	0.60
3, xyloside	29.7 ± 0.2	<10		0	0	1564	0.85
4, rhamnoside	27.5 ± 0.0	<10		1	0	1554	0.60
5, maltoside	29.3 ± 0.2	<10		1	0	1552	0.44
6, dimethylated maltoside	26.9 ± 0.2	44	21	45	19	1550	0.37
7, maltotrioside	29.3 ± 0.2	<10		17 → 9	0	1547	0.33
8, hydroxyethyl	24.6 ± 0.4	27	19	28	18	1563	1

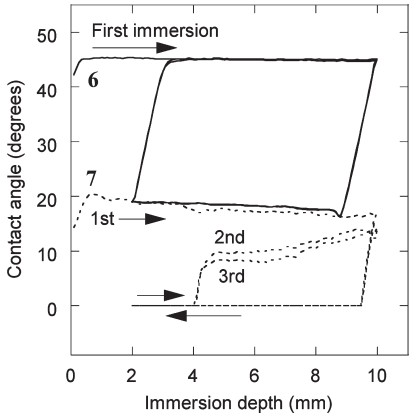

Figure 2. Contact angles for the dimethylated maltoside (**6**, solid lines) and maltotrioside (**7**, dotted lines) as determined by the Wilhelmy method. Three complete wetting/dewetting cycles are shown for each sample. The receding contact angle for **7** is zero in all cycles, and because of hysteresis, the advancing angle is zero for the first 2 mm on the second and third wetting cycles (i.e., between 2 and 4 mm in the diagram).

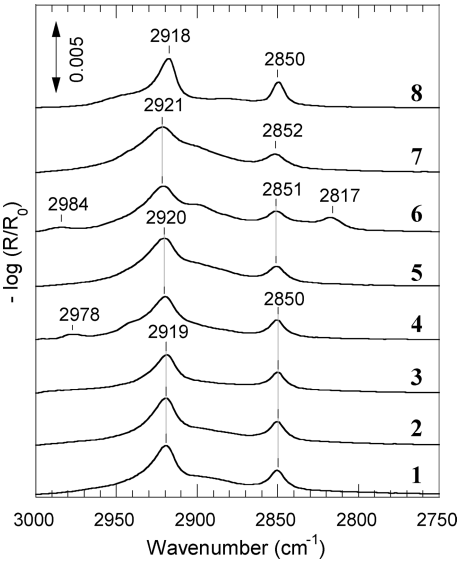

Figure 3. RA spectra in the C−H stretching region of saccharide-terminated alkanethiolate SAMs.

contact angles were also analyzed by the Wilhelmy method using a tensiometer. The results for the quantifiable goniometric contact angles of **6** and **8** are in good agreement with the tensiometry data (Table 1), and for the monosaccharides and **5**, the tensiometric data do not provide much additional information even though figures can be assigned to the contact angles. For **1**−**5**, the immersion cycles are featureless, with the wetting and dewetting legs of the cycles virtually indistinguishable. **6** and **8** have significant hysteresis. However, they are well-behaved in the sense that the repeatability between cycles is very good. (See the data for **6** in Figure 2.) This is not the case for maltotrioside **7**, where although the receding contact angles are zero in every dewetting cycle the advancing contact angle is both decreasing for every additional cycle and changing irregularly within each immersion, indicating a saturation effect or a slow rearrangement of the surface, which is not completely reversible on the timescale of the measurement. This is evidence of considerable disorder in the maltotrioside layer.

The contribution to the thickness from a single saccharide unit is estimated to approximately 3 Å from comparison with **8**, consisting only of a hydroxyethyl group (Table 1). A thickness of ~27.7 Å was observed for **1**, **2**, and **4** and 29.7 Å for **3**. This difference is due to both the variations in the conformation and the tilt angle of the alkane chain and improved packing of the headgroups as a result of reduced steric hindrance from the relatively planar configuration of the sugar moiety in **3**. Although the increased thickness of disaccharide SAM **5** compared to that of the monosaccharides is less than 3 Å, the increment due to the addition of the extra sugar ring is significant. However, dimethylated maltoside **6** shows nearly no increase in thickness compared to the SAMs containing monosaccharides. This demonstrate how sensitive the molecular packing is to small changes in the molecular structure, where a change in headgroup interactions or steric hindrance from the two additional methyl groups reduces the molecular packing, increases the SAM disorder, and reduces the total thickness. The contact angles on the two SAMs show that **5** is a completely wettable surface whereas **6** is much less hydrophilic. It is interesting to compare the wettabilities of **6** and **4**, where the complete wetting of **4** suggests that its methyl group, although being located close to the SAM surface, is not sufficiently exposed to the surrounding medium (i.e., shielded by

dx.doi.org/10.1021/la202774e |*Langmuir* 2011, 27, 15034–15047

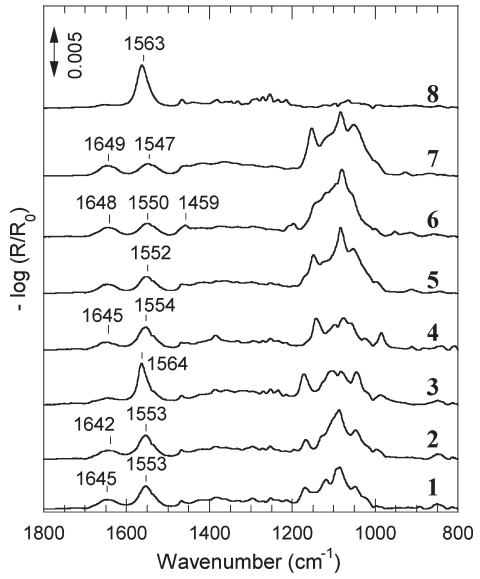

Figure 4. RA spectra in the amide and the fingerprint regions of saccharide alkanethiolate SAMs.

hydroxyl groups), indicating that **6** has a more loosely packed structure. Furthermore, comparing the wettability of **4** with that of a monomethylated galactopyranoside ($\theta_a = 52°$, $\theta_r = 22°$)[13] demonstrates that a small change in the carbohydrate structure may result in considerable differences in the wettability, representing differences in the molecular packing. The thickness of trisaccharide **7** was found to be the same as that for disaccharide **5** (and monosaccharide **3**), which, in view of the contact angle tensiometry results discussed above, clearly is the result of disorder in the molecular packing caused by the bulky carbohydrate moiety, as is also confirmed by the IRAS data discussed below.

Infrared Reflection−Absorption Spectroscopy. Infrared reflection−absorption spectroscopy was used to obtain specific information about the alkane chain orientation and the molecular order of the monolayer on the gold surface. Reflection−absorption (RA) spectra in the C−H stretching region of the saccharide alkanethiols on gold are presented in Figure 3.

C−H Stretching Region. The C−H stretching region (between 3000 and 2800 cm^{-1}) provides information about the molecular packing and crystallinity of the alkyl chains in the monolayer. For a perfectly ordered all-trans arrangement of alkyl chains, the absorptions will appear at 2918 (d^-) and 2850 (d^+) cm^{-1}.[29,30] In Figure 3, the RA spectra show the asymmetric methylene C−H stretching from the alkyl segment at 2919 cm^{-1} for **1**, **2**, and **3**, shifted to 2920 cm^{-1} for **4** and **5** and finally located at 2921 cm^{-1} for **6** and **7**. The shift to higher frequencies of the peak of this band indicates a slight increase in the number of gauche defects along the alkyl chain due to the increasing size and bulkiness of the saccharide-termini, causing molecular chain packing disorder. For the same reason, the corresponding frequencies of the symmetric methylene C−H vibration exhibit a shift from 2850 to 2852 cm^{-1}. The increasing disorder with increasing complexity (size) of the terminal saccharide groups is also reflected in an overall broadening of the C−H vibrational peaks. In the SAMs of **4** and **6**, there are additional vibrations in this region originating from methyl C−H stretching in the saccharide moieties. They appear at 2984 (r^-), 2817 (r^+), and ca. 2900 cm^{-1} in **6** and at 2978 (r^-) cm^{-1} in **4**, depending on the substituent to which the methyl group is attached.[31]

Amide Bands. The amide bond in the molecules form lateral hydrogen bonds that stabilize the overall SAM structure.[32] In Figure 4, both the amide I band (predominantly C═O stretching) and the amide II band (C−N stretching combined with C−N−H in-plane bending) can be seen at ∼1645 and ∼1550 cm^{-1}, respectively. According to the surface selection rule, the infrared absorption of a vibrational mode of a molecule on a metal surface is determined by the projection of its transition dipole moment on the surface normal. Because of the interaction of the dipole moment of the molecule with its image charges, dipole moments parallel to the surface cancel while dipole moments perpendicular to the surface are amplified. Therefore, the corresponding intensity of a vibrational mode in the spectrum is strongly dependent on the molecular orientation relative to the surface. Among the investigated SAMs, **3** displays a considerably strong, sharp amide II absorption at 1564 cm^{-1} and the near absence of the amide I absorption (∼1645 cm^{-1}). This observation indicates that the orientation of the carbonyl group (amide I) in **3** is predominantly aligned parallel to the gold surface and that the C−N bond (amide II) is close to parallel to the surface normal. Consequently, the preferential orientation of the alkane chains in **3** is nearly parallel to the surface normal. Comparing this result with the amide bands of the other SAMs, we find that **3** is oriented in a more upright direction, resulting in a thicker layer, in agreement with the ellipsometric data (shown in Table 1). Beside the tendency of the amide II peak intensity to decrease in response to increased disorder, there is also a shift of the peak position to lower frequencies with larger carbohydrate termini. This shift has contributions from the increased effective mass of the nitrogen atom coupled to the bulky end group, but it is dominated by the strength of the NH···O═C hydrogen bond.[33,34] As the strength of the hydrogen bond increases, the amide II peak shifts to higher frequencies, and because the in-plane hydrogen bonding of neighboring amides is an indicator of SAM order, these peak positions are also of interest. The amide II peak positions are included in Table 1 for the single-component SAMs, and it is clear that monosaccharide **3** is distinctly different from all the other saccharides in that the peak position is at least 10 wavenumbers higher and very similar to that of hydroxyethyl-terminated **8**, providing strong support to the hypothesis that **3** is more ordered than the other monosaccharides and that this is the cause of the difference in SAM thickness. Beside **3**, the data in Table 1 shows a clear trend toward decreasing frequency of the peak position as the size of the saccharide moiety increases, again in agreement with the observed increase in disorder of the SAMs.

Fingerprint Region. The frequencies between 1200 and 950 cm^{-1} in the RA spectra provide conformational information about C−O, C−C, C−H, and O−H vibrational modes of the saccharides. This results in a multitude of partially overlapping bands, rendering complex spectra that are very difficult to interpret in detail (Figure 4). The absorptions observed at ∼1050, ∼1080, ∼1100, ∼1150, and ∼1170 cm^{-1} are assigned to C−O−C vibrations of the carbohydrate ring; the intensity and peak position vary with the saccharide structure.[12] Furthermore, the weak absorptions of methylene C−H scissoring at ∼1467 cm^{-1} and methyl C−H bending at around 1385 cm^{-1} can also be discerned in the spectra.

Mixed SAMs. To improve the control of the interfacial properties of the SAMs and also to increase the availability of the sugar moieties, we dilute the saccharide-functionalized thiols with a hydroxyethyl-functionalized filler molecule (**8**). Thus, for the SAMs where the bulkiness of the headgroup is observed to

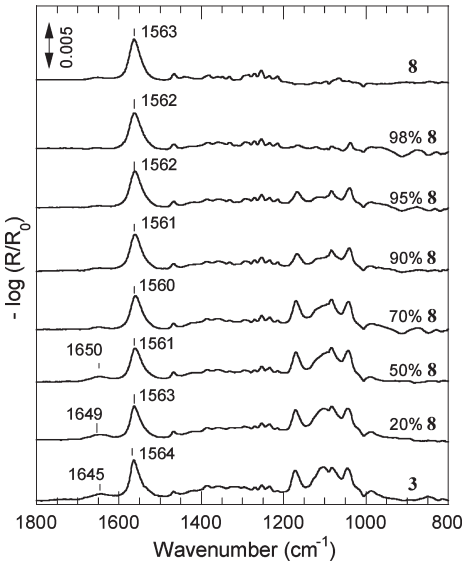

Figure 5. RA spectra of the fingerprint region of mixed xyloside (**3**)/hydroxyethyl filler (**8**) SAMs.

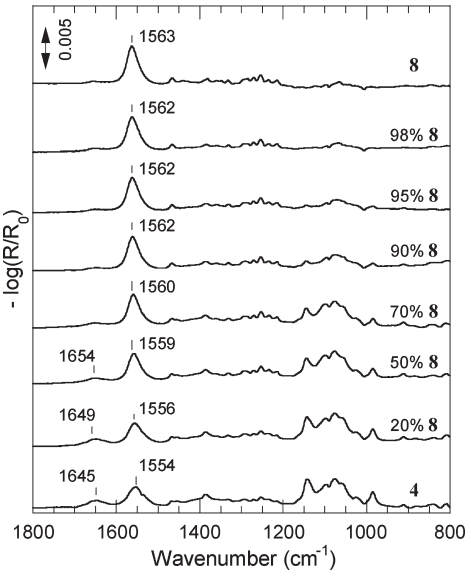

Figure 6. RA spectra of the fingerprint region of mixed rhamnoside (**4**)/hydroxyethyl filler (**8**) SAMs.

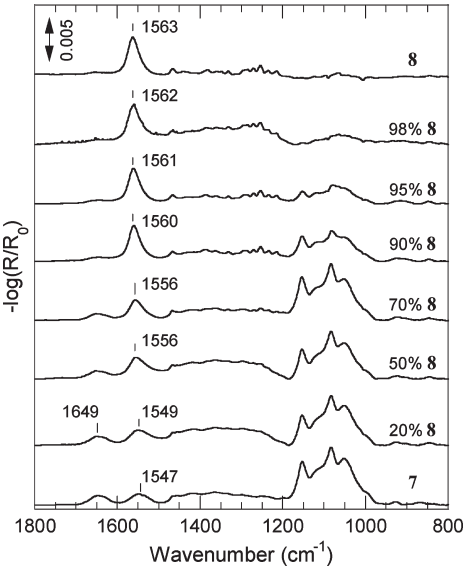

Figure 7. RA spectra of the fingerprint region of mixed maltotrioside (**7**)/hydroxyethyl filler (**8**) SAMs.

reduce the molecular packing in the SAM, mixed monolayers are expected to improve the alkyl chain order and for some range of dilutions (depending on the saccharide headgroup) also improve the molecular packing of the sugars simply by bringing the bulky saccharide termini further apart. We examine mixtures of the xyloside (**3**), rhamnoside (**4**), and maltotriose (**7**) molecules with filler molecule **8** in different molar ratios. It is anticipated that the saccharide moieties of these molecules pack differently in the monolayer because of differences in steric hindrance. The order in the xyloside monolayer (**3**) is not expected to be greatly improved by dilution with filler molecules because the xylose ring is relatively planar. This is in contrast to the rhamnoside (**4**), which has a markedly nonplanar character, and the maltotriose (**7**) headgroup whose bulkiness is clearly a severe constraint to the packing in the SAM. The RA spectra of the amide and fingerprint regions of these mixed SAMs are shown in Figures 5−7. In the C−H stretching region, a shift from 2919 to 2918 cm^{-1} of the C−H asymmetric stretching band is observed when mixing **3** with 20% or more of the filler molecule (not shown, available as Supporting Information). As mentioned previously, the position of this absorption is a signature of an all-trans arrangement of the alkane chains, which indicates a slight improvement in methylene packing with >20% **8** in this SAM. The amide II peak positions for different dilutions are shown in Figure 8a, and it is seen for mixtures of **3** with **8** that there is an initial decrease in the peak frequency and a minimum between the single-component compositions. Although this is not in complete agreement with the shift in the asymmetric C−H stretching, the effects are relatively small. For the mixed systems of **4** and **7**, filler molecule **8** needs to be added to at least 50% in order to obtain an all-trans arrangement of the alkane chain in the mixed system (as determined from the C−H stretching peak positions; see Supporting Information). Amide II peak shifts with increasing dilution by **8** show a clear, continuous trend toward increasing alkane chain order as the fraction of **8** is increased in the SAM (Figure 8a). Changes in the surface coverage of the carbohydrate moiety in the mixed SAM systems were obtained by area integration over the frequencies between 1200 and 950 cm^{-1}. From Figure 8b, it can be inferred that to reduce the surface coverage of saccharides to half the original value the addition of between 70 and 80% filler molecule to the mixtures must be made, although it should be mentioned that the orientation of the terminating carbohydrate moiety also affects the calculated intensities so that the change in orientation of the saccharide with surface coverage introduces an additional uncertainty into these numbers. It is also notable that the integrated intensity decreases continuously for **3** as **8** is added, showing that as the SAM is diluted with filler molecule **8** so also are the saccharide moieties, as would be a consequence of dilution of an already well-packed layer. This is not the case for **4** and **7**, where the surface coverage of sugar groups is relatively constant up to filler fractions of approximately 50%, which means that up to a 50% mixture the filler appears to fill up the alkane part

dx.doi.org/10.1021/la202774e |*Langmuir* 2011, 27, 15034–15047

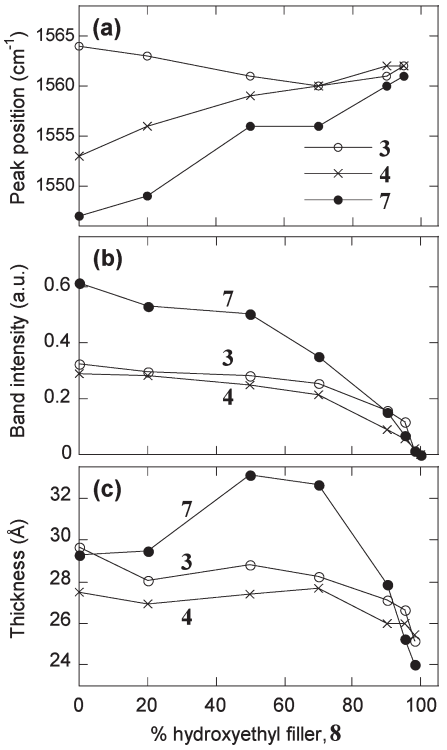

Figure 8. (a) Amide II peak positions, (b) saccharide surface coverage, as inferred from area integration of the IRAS spectra in the fingerprint region (1200−950 cm^{-1}), and (c) ellipsometric thicknesses for the mixed monolayers where the rhamnoside (**3**, ○), xyloside (**4**, ×), and maltotrioside (**7**, ●) have been mixed in various ratios with the hydroxyethyl (EG1)-terminated filler molecule (**8**). For clarity, lines connect data points for each sample.

of the monolayer and that the surface coverage of saccharides is still limited by packing constraints in the saccharide layer over this concentration range. This is supported by the ellipsometric thicknesses of the mixed SAMs, shown in Figure 8c. For **3**, there is a decrease in thickness as filler molecules dilute the layer. For **4**, the thickness is relatively constant up to about 70% dilution, but for **7**, there is a significant increase in the total thickness as the fraction of the filler molecule is increasing, with a maximum thickness of 33.1 Å at 70% **8** content compared to 29.3 for the single-component **7** layer. The thickness variation is more pronounced for **7** than for **4** because with the former it can be expected that the initial degree of disorder in the alkane chain layer is significantly higher. The change in amide band intensities is also of interest for the characterization of the change in structure upon dilution with the filler molecule. The spectrum for the single-component **8** SAM (Figure 5) has a strong amide II intensity and a barely visible contribution from the amide I band, demonstrating that the alkane chains have a nearly upright conformation and that the amide carbonyl is oriented parallel to the gold substrate. The difference between the amide band structures of **3** and **8** is small, confirming our expectation that the xyloside functionalities do not severely impede the packing of the alkane chains in the monolayer. However, in looking at the RA spectra for the mixture of **8** with either **4** or **7** (Figures 6 and 7), we find that the situation is different; the amide II intensity for pure **4** SAMs is weak and that for pure **7** SAMs is even weaker, but in both cases, the intensity approaches that of the pure filler SAM at about 70%, in good agreement with the conclusions

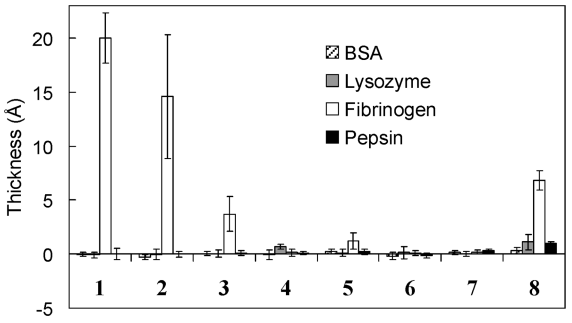

Figure 9. Ellipsometric thicknesses of the adsorbed protein layers. In each case, the protein solutions were 1 mg/mL protein in PBS. Error bars show the standard deviation.

drawn from the integrated areas in the fingerprint region. At filler fractions of up to 70%, the order of the alkane chain layer is improved as available space is filled beneath the sterically constrained layer of saccharide moieties. At higher filler fractions, we start diluting the saccharide moieties, and further increases in the filler fraction do not improve the packing or the order in the alkane chain layer.

Protein Adsorption Results. The proteins used in the protein resistance tests were chosen to cover a range of sizes from 14 to 340 kDa for lysozyme and fibrinogen, respectively, globular (e.g., BSA) versus nonglobular (fibrinogen) proteins, and surface charge properties from the pI 2.9 of pepsin to lysozymes' pI 11. Albumin and fibrinogen are among the most prevalent plasma proteins, and the latter is widely studied because of its role in coagulation and platelet adhesion.[35] The results of the protein adsorption tests are shown in Figure 9. There was very little adsorption of bovine serum albumin (BSA), lysozyme, or pepsin to any of the surfaces. Fibrinogen behaved differently, adsorbing to several of the SAMs in significant amounts. However, there were clear differences between the surfaces in this respect. A very dramatic trend in decreasing fibrinogen adsorption can be seen for the monosaccharide series **1** > **2** > **3** > **4**. However, we do not see any correlation between the variation in fibrinogen adsorption with any of the physicochemical parameters that have been determined for the surfaces, be it thickness, wettability, wetting hysteresis, or the molecular order in the alkyl chain or headgroup regions. It is also notable that the other tested proteins were unaffected by these variations. The fact that fibrinogen behaves so differently from the other proteins is not surprising; it is well known that fibrinogen has a higher propensity to adsorb to surfaces in greater quantities and to adhere more strongly than most other proteins.[36,37] Although we cannot exclude that specific interactions between fibrinogen and these monosaccharides are responsible for the high adsorption, this is very unlikely because of the limited steric availability of the sugar moieties in the close-packed monolayer. In any case, rhamnose-terminated **4** appears to be very protein-resistant under these conditions, which is also true for the tested disaccharides (**5** and **6**) and the trisaccharide (**7**). These SAMs have in common that they are more disordered than surfaces **1**−**3** and **8**, where fibrinogen adsorption is non-negligible. The result for **8** is in agreement with what is known about fibrinogen adsorption onto OEG-terminated SAMs; terminating EG_1 and EG_2 units are too short to provide protein-resistant surfaces, whereas this is achieved with SAMs having EG_3 or longer termination.[38,39] For the monosaccharides, the situation is more difficult; we have demonstrated in previous

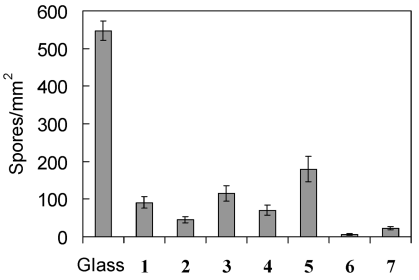

Figure 10. Results of the *Ulva* assay for the seven saccharide SAMs and a Nexterion glass slide used as an internal laboratory control. $N = 90$, error bars = $\pm 2 \times$ standard error.

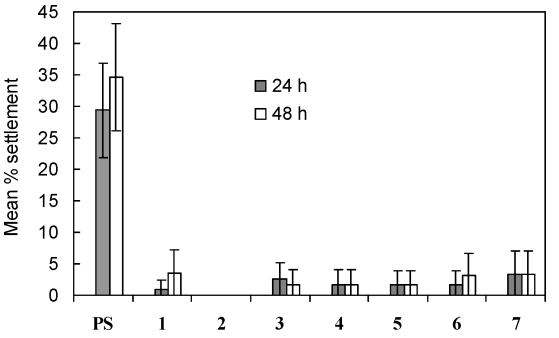

Figure 11. Barnacle assay results for the seven SAMs and for a polystyrene surface used as an internal laboratory standard to verify the viability of the cypris larvae and that the settlement behavior was normal. The results are shown as the percentage of settled cyprids, with 95% confidence intervals.

studies that monosaccharide SAMs may show very good protein[12] and marine biofouling[13] resistance. However, these studies also show that small variations in the structure of the sugar moieties may be decisive for the antifouling behavior. A related observation was published recently, where protein adsorption onto chiral polyol SAMs was studied, and it was found that adsorption onto either of two enantiomers was higher than adsorpion to the racemic mixture; this difference was speculated to be caused by variations in water solvation at the interfaces.[16] We do not currently have detailed-enough information about the monosaccharide SAMs to make any claims about the cause of these differences, so we have to leave this to future work.

In comparing **2**, **5**, and **7**, which consist of one, two, and three glucose units, respectively, we at least note that there is a clear trend toward increasing resistance to fibrinogen adsorption with a greater number of glucose units in the chain. The main effect that this variation has on the monolayers is a decrease in order in the SAMs whereas the total layer thickness changes only marginally. Despite the differences in the size of the headgroup, the change upon going from monosaccharide **2** to disaccharide **5** is only 1.4 Å but di- and trisaccharides **5** and **7**, respectively, have the same thickness, and it appears that the increased disorder of the layers could be of relevance. An early study on the protein resistance of OEG-terminated alkylthiols diluted with methyl-terminated thiols concluded that protein resistance was preserved at higher fractions of methyl-terminated thiols if the OEG chains were longer, thus suggesting that the surface coverage of the EG units is critical.[40] It appears that a similar relation between coverage and resistance holds for the set **2**, **5**, and **7**. In either case, we suggest that oligosaccharide-terminated SAMs will be interesting for further investigations of antifouling properties.

Marine Fouling Assays. To test the resistance of these SAMs to marine biofouling, we performed experiments with two model organisms: the zoospores of the alga *Ulva linza* and cypris larvae of the barnacle *Balanus amphitrite*. In both assays, the number of spores or larvae attached to the test surfaces was quantified. The adults of these two species are common macrofoulers in marine environments.

Ulva Assays. The density of spores attached to Nexterion glass and seven oligosaccharide SAM surfaces is shown in Figure 10. Nested one-way ANOVA showed no significant difference between the oligosaccharide surfaces ($p = 0.05$). Further statistical analysis showed that the density of spores on all of the oligosaccharide surfaces was significantly lower than on the glass, demonstrating that spores did not settle indiscriminately (Dunnett's posthoc test[41]). The data concurs with previous data for hydrophilic surfaces, including mixtures of (OH/CH_3)-terminated SAMs[42] and xerogels[43] where spore settlement was low on all surfaces until the water contact angle was >50°. Similar results were also found in relation to the increasing wettability of hexa(ethylene glycol) SAMs with different alkoxyl end-group terminations.[44]

Barnacle Assays. All SAM surfaces resulted in very small, or negligible, settlement of barnacle cyprids (Figure 11). That this is not a result of defective larvae is demonstrated by the included result for an internal laboratory polystyrene (PS) standard, evaluated in parallel with the SAMs. As well as settlement, a note was made of the numbers of "dead" cyprids and the percentage mortality was calculated; no abnormal behavior was noted.

The variation in cyprid settlement among samples **1**−**7** is small, and statistical analysis does not show any significant differences in the group ($p < 0.05$). This is also in agreement with the previous observation that saccharide SAMs with widely varying properties (e.g., water contact angles ranging from <10 to 76°) were equally unappealing to cypris larvae.[13] It is tempting to speculate that there is some optical property of the gold substrate that universally deters cyprids from the surfaces, though because the settlement assays are performed in the dark it is difficult to see what this could be. An analysis of the exploratory behavior of cypris larvae on the saccharide surface may reveal differences in the pattern of searching as shown for two settlement-inhibiting zwitterionic surfaces.[45]

■ CONCLUSIONS

An efficient strategy for the synthesis of diverse glycosyl-terminated alkanethiols from often readily available 2-azidoglycoside in a four-step manner has been explored. The outlined route shows promise in multigram-scale syntheses because of the relatively low complexity in the used reaction methods. We have also established an effective route to derive 6,6′-*O*-dimethylated maltosyl analogue **6**.

The structure of SAMs formed on gold substrates from the produced thiols was investigated, and it was demonstrated that the SAM structure, particularly evaluated as order in the alkyl chain layer, was dependent on the conformation of the monosaccharide moieties. The relatively planar structure of the xyloside (**3**) permits close packing and results in a well-ordered layer structure, and the markedly nonplanar rhamnoside (**4**) constrains the packing and results in a less-ordered SAM. As the headgroups become more bulky, as in the case of di- and trisaccharides, the structural qualities are further reduced, resulting in increasing

disorder in both the headgroup and alkyl chain regions as compared to that in the monosaccharide SAMs.

Saccharide-terminated SAMs have previously shown promising antifouling properties in both protein adsorption studies and in marine biofouling laboratory assays, and we thus subjected the SAMs described in this article to similar tests to evaluate their antifouling properties. We note that the SAMs are overall very resistant to the tested proteins, with the exception of fibrinogen. Fibrinogen adsorption varies considerably for the four tested monosaccharides in a way that we are not able to correlate with any of the studied physicochemical properties of the SAMs. Including also the di- and trisaccharide SAMs in a comparison of fibrinogen adsorption, we note that there is a trend for less-ordered monolayers to be more resistant to fibrinogen adsorption. The attachment of both algal zoospores and barnacle cypris larvae was low on all of the tested SAMs. Attachment was significantly lower on the SAMs than on the laboratory standards (glass and polystyrene), but differences among the SAMs were not statistically significant.

Thiols with bulky sugar moieties produce disordered monolayers. For these, the packing of the alkyl chain layer can be improved by dilution with a filler molecule having a small headgroup, whereas the total number of saccharide moieties on the surface is kept relatively unchanged for surface dilution up to approximately 50%. We also note that further dilution of the saccharides on the surface is a useful strategy for improving the accessibility and exposure of the saccharide headgroups to the environment and thus also for optimizing specific interactions of proteins or cells with surface-bound sugars. The good resistance to the nonspecific fouling of our SAMs supports the viability of this approach and also suggests that further work with oligosaccharide SAMs could be of considerable interest in understanding fouling resistance and the development of antifouling coatings.

EXPERIMENTAL SECTION

Gold Substrate Preparation. Silicon (100) wafers with native oxide were cut into pieces (10×19 mm^2 for protein adsorption experiments or 20×40 mm^2 for IRAS); $12.5 \times 20 \times 0.15$ mm^3 glass coverslips were used for Wilhelmy measurements. All substrates were TL1 cleaned (immersed in a 5:1:1 mixture of water, 30% H_2O_2 (Merck), and 25% NH_3 (Merck) for 10 min at 85 °C). After being cleaned, they were carefully rinsed with water (all water was Milli-Q water (Millipore)) and moved to a laminar flow cabinet, dried with nitrogen gas, and mounted in a UHV electron-beam evaporation system (Balzers UMS 500 P) operating at a base pressure of 10^{-9} mbar and an evaporation pressure of about 10^{-7} mbar. A 25 Å titanium adhesion layer (Balzers, Liechtenstein, 99.9%) was deposited at a rate of 2 Å/s, followed by a 2000 Å gold layer (Nordic High Vacuum AB, Sweden, 99.9%) at 10 Å/s. Glass coverslips (12.5×20 mm^2) for Wilhelmy plate measurements of contact angles were coated on both sides.

Samples for *Ulva* assays were prepared on cleanroom-cleaned 76×25 mm^2 Nexterion Glass B slides (Schott) and treated like other samples, except for the metal coating that was carried out in a resistively heated vacuum evaporation system with a base pressure of $<4 \times 10^{-6}$ mbar using a 25 Å chromium adhesion layer (at 0.4−0.6 Å/s) and then 2000 Å of gold (at 5−10 Å/s). Samples for barnacle assays were prepared in 24-well cell culture plates, the wells of which were coated on the inside by mounting them at a variable angle on a rotating sample holder, and then evaporated in the resistively heated system under the conditions described above while gradually varying the angle of the plate so as to cover both the side and the bottom of the wells. The plates were sterile when mounted, and to avoid the TL1 cleaning steps, the wells were filled with the thiol solutions immediately after removal from the evaporator.

Self-Assembled Monolayer Preparation. All SAMs were prepared from solutions with a total thiol concentration of 50 μM in ethanol (99.5%, Kemetyl, Sweden). Solutions for mixed SAMs were prepared by volumetrically mixing 50 μM solutions of the individual components to the desired molar ratio. (All molar ratios refer to solution concentrations. Note that the molar ratio in the mixed SAM does not necessarily agree with the solution ratio.) All solutions were stored at room temperature in polypropylene jars (Nalgene) that had been previously rinsed and ultrasonicated for 15 min in hexane (Merck) and 15 min in ethanol. Prior to SAM adsorption, gold substrates were TL1 cleaned twice, rinsed with water, and dried with nitrogen. Optical characteristics of the gold substrates were obtained by ellipsometry immediately after cleaning. The substrates were incubated for at least 20 h in the thiol solution (exactly 24 h for mixed SAMs). They were then removed from the thiol solutions, rinsed with 99.5% ethanol, ultrasonicated for 5 min in ethanol in order to remove any physisorbed thiols, dried with nitrogen, and immediately analyzed using ellipsometry and/or contact angle measurements and infrared spectroscopy.

Ellipsometry. Ellipsometry was performed using an automatic Rudolph Research AutoEL ellipsometer (using a He−Ne laser, λ = 632.8 nm, set at a 70° angle of incidence). The measurements were carried out using an automatic program that measured five different points on each sample and used the average. The necessary optical constants were obtained from the measurements of the gold substrates immediately after cleaning, as described above. A three-phase air/organic film/gold model was used to calculate the thickness of the SAMs, assuming an isotropic, transparent organic layer. The refractive index of the organic film (SAM as well as protein) was assumed to be 1.5.

Contact Angle Goniometry. A semiautomatic optical contact angle meter (KSV CAM 200) was used to determine the advancing and receding contact angles of water on the SAMs. A manual dispenser was used to expand or retract a droplet on the sample. As the droplet was expanded, images were acquired for the evaluation of advancing contact angles; similarly, receding contact angles were determined from images acquired as water was withdrawn from the droplet into the syringe. During the measurements, the syringe needle was kept inside the center of the drop, and a high-speed CCD camera was used for image capture. The images were analyzed using the software supplied with the instrument.

Contact Angle Tensiometry. For more accurate measurements of these very hydrophilic SAMs, contact angles of single-component SAMs were determined using a Wilhelmy balance (Sigma 70, KSV). The glass coverslips were suspended from the balance, and the movement of the water reservoir was set to a speed of 5 mm/min and a 10 mm maximum immersion depth. Three cycles were carried out for each sample, cycling only the lowest 8 mm of each sample, and shown values of the contact angles are the averages of the three cycles, ignoring the values obtained over the first 2 mm after each turning point. The instrument control program calculates the wetting force and the contact angle during the instrument operation, using the known dimensions and density (2.29 g/cm^3) of the glass coverslips (including the thickness in the periphery) and a measured value of the water surface tension. This was determined immediately before the contact angle measurement using a platinum Wilhelmy plate (19.6 mm wide and 0.1 mm thick). Ten immersion cycles were used for each surface tension data point; measured values always exceeded 72.2 mN/m.

Infrared Reflection−Absorption Spectroscopy. Reflection−absorption (RA) spectra were recorded on a Bruker IFS 66 system equipped with a grazing angle (85°) infrared reflection accessory and a liquid-nitrogen-cooled MCT detector. The sample chamber was continuously purged with nitrogen gas during the measurement. All spectra were acquired at 2 cm^{-1} resolution between 4000 and 700 cm^{-1} as a

summation of 3000 scans. A three-term Blackmann−Harris apodization was applied to the interferograms before Fourier transformation. The background spectrum (R_0) was taken using a deuterated hexadecanethiolate [$HS(CD_2)_{15}CD_3$] SAM on gold. This ensures that the surface is free of hydrocarbons, which otherwise tend to contaminate clean gold surfaces quickly and interfere with the studied C−H stretching bands. The sample spectrum (R) was acquired under identical equipment conditions and compared to the background spectrum to obtain $-\log(R/R_0)$ versus reciprocal centimeters. Prior to the IRAS measurement, the monolayer sample was removed from the incubation solution, thoroughly rinsed, ultrasonicated, rinsed again with ethanol, and finally dried in flowing nitrogen gas.

Protein Adsorption Experiments. Phosphate-buffered saline (PBS; 10 mM sodium hydrogen phosphate Na_2HPO_4, 10 mM potassium dihydrogen phosphate KH_2PO_4, and 150 mM NaCl in water) was adjusted with NaOH to pH 7.4. The protein solutions were prepared by dissolving 1 mg/mL of the respective protein in PBS. Shortly before incubation in protein solutions, the SAMs were rinsed with water and dried with nitrogen, and the SAM thickness was determined by ellipsometry. After this measurement, the samples were incubated in 7 mL of the protein solutions at room temperature. After 30 min, samples were removed from the protein solutions, placed in a beaker with PBS for 10 min, rinsed with water, and dried with nitrogen. New ellipsometry measurements were then performed, following the previously described procedure, and the thickness increments (Δ thickness) were calculated.

***Ulva* Assay.** Reproductive thalli of green macroalga *Ulva linza* were collected from Llantwit Major beach, Glamorgan, Wales (52° 23′ N, 3° 30′ W). Zoospores were released into artificial seawater (ASW) at pH 8.0 and 32‰ ("Tropic Marin", Aquarientechnik GmbH) and prepared for assay as described previously.[46] SAMs were stored and shipped under nitrogen, assayed within 24 h of receipt, and in contact with air for less than 5 min before the assay. Settlement assays followed the principles outlined in Callow et al.[46] and Finlay et al.[47] In brief, each surface was placed in a separate compartment of a Quadriperm dish (Greiner Bio-one Ltd.) to which 10 mL of a suspension containing 1.5×10^6 mL^{-1} zoospores was added. Zoospores were allowed to settle for 1 h in the dark before the residual suspension was aspirated and the slides were gently washed. The motility of the aspirated zoospores was assessed by virtue of their negative phototaxis; viable spores retain their motility. Slides were then fixed in 2.5% (v/v) glutaraldehyde, washed, and air-dried. The density of settled (adhered) spores was determined using an epifluorescence microscope with an image analysis system (Zeiss Kontron 3000).[48] Thirty fields of view were counted at 1 mm intervals along the length of each of three replicates slides.

Barnacle Assay. The 24-well plates were rinsed gently with artificial seawater (ASW) to remove any remaining solvents and then placed into ASW for 1 h before the assay was started. Briefly, 10 3-day-old cyprids were introduced into each well contained within 2 mL of ASW. The plates were incubated at 28 °C for 24 h. After this period, each plate was inspected to obtain the percentage settlement. After another period of 24 h, the plates were again inspected to determine the settlement after 48 h. A blank 24-well plate (polystyrene) was included in the assay as an internal laboratory standard to gauge the settlement behavior of the cyprids and to act as a control. The results are expressed as the percentage of the settlement, with 95% confidence intervals. The data were analyzed statistically using the Kruskal−Wallis test with post hoc comparisons of treatment means made with the Dunn's multiple comparison test.

General Synthesis Methods. Organic phases were dried over $MgSO_4$ (s), filtered, and concentrated in vacuo at 40 °C. Thin layer chromatography (TLC) was performed on silica gel plates (Merck F_{254} plates) with detection by charring with AMC [ammonium molybdate 10 g, cerium(IV) sulfate 2 g, dissolved in 10% H_2SO_4 (200 mL)] or PAA [EtOH (95%, v/v)/H_2SO_4/*p*-anisaldehyde/acetic acid 90:3:2:1] followed by heating to ∼250 °C. Flash chromatography (FC) was performed with silica gel (Sigma-Aldrich, 0.040−0.063 mm). NMR spectra were recorded on a Varian Mercury 300 (^{1}H 300 MHz and ^{13}C 75.4 MHz) instrument at 25 °C in $CDCl_3$, MeOH-d_4, or DMSO-d_6. Chemical shifts are given in ppm relative to solvents peaks[49] in $CDCl_3$ (δ 7.26 for ^{1}H and δ 77.16 for ^{13}C), MeOH-d_4 (δ 3.31 for ^{1}H and δ 49.00 for ^{13}C), and DMSO-d_6 (δ 2.50 for ^{1}H and δ 39.52 for ^{13}C). FT-IR spectra were recorded as KBr pellets (solids) on a Perkin-Elmer Spectrum 1000 FT-IR spectrometer. Optical rotations were recorded at room temperature with a Perkin-Elmer 41 polarimeter. MALDI-TOF mass spectra were recorded with a Voyager-DE STR Biospectrometry workstation, in positive mode, using a α-cyano-4-hydroxycinnamic acid matrix. High-resolution mass spectra were recorded by *i*Novacia AB, Stockholm. Filler molecule **8** was synthesized as described previously.[22]

(*S*-Acetyl)-*N*-(16-mercapto-palmitoyl)-2-aminoethyl-2,3,4-tri-*O*-acetyl-α-L-rhamnopyranoside (4b). A mixture of peracetylated 2-azidoethyl-α-rhamnoside (**4a**) (0.275 g, 0.765 mmol) and Boc_2O (0.250 g, 1.148 mmol) was dissolved in absolute EtOH (3 mL) and hydrogenated for 22 h using palladium on carbon (50 mg, 10%) under vigorously stirring and H_2 (1 atm). The suspension was filtered and concentrated. The obtained syrup was treated with TFA (1 mL) in dry CH_2Cl_2 (5 mL) for 4 h at ambient temperature, quenched with MeOH (1 mL), and coevaporated with toluene. Crude amino sugar, **9** (0.425 g, 0.995 mmol) and DIPEA (0.150 mL, 0.842 mmol) were stirred in dry DMF (10 mL) for 6 h and coevaporated with toluene. FC (toluene/EtOAc 1:1) gave **4b** (0.325 g, 0.503 mmol, 66%) as a white solid. R_f = 0.36 (toluene/EtOAc 2:1). $[\alpha]_D$ = −30 (*c* 1.0, $CHCl_3$). IR ν_{max} cm^{-1}: 3315, 2921, 2849, 1748, 1695, 1647, 1558, 1468, 1373, 1247, 1224. ^{1}H NMR (300 MHz, $CDCl_3$): δ 1.21 (d, 3 H, *J* = 6.3 Hz), 1.23−1.35 (m, 22 H), 1.50−1.57 (m, 2 H), 1.59−1.64 (m, 2 H), 1.98 (s, 3 H), 2.03 (s, 3 H), 2.14 (s, 3 H), 2.19 (t, 2 H, *J* = 7.7 Hz), 2.30 (s, 3 H), 2.85 (t, 2 H, *J* = 7.3 Hz), 3.35−3.43 (m, 1 H), 3.45−3.51 (m, 2 H), 3.72−3.78 (m, 1 H), 3.82 (dq, 1 H, *J* = 6.3, 9.6 Hz), 4.72 (d, 1 H, *J* = 1.1 Hz), 5.05 (dd, 1 H, *J* = 9.6, 9.6 Hz), 5.28−5.23 (m, 2 H), 5.86 (bs, 1 H). ^{13}C NMR (75.4 MHz, $CDCl_3$): δ 17.5, 20.8, 20.9, 21.0, 25.9, 28.9, 29.2, 29.3, 29.5−29.7 (several peaks), 30.7, 36.9, 39.0, 66.7, 67.3, 69.2, 69.8, 71.1, 97.7, 170.0, 170.2, 170.3, 173.4, 196.1. HRMS: $[M + H]^+$ calcd for $C_{32}H_{55}NO_{10}S$, 646.3619; found, 646.3632.

***N*-(16-Mercapto-palmitoyl)-2-aminoethyl-α-L-rhamnopyranoside (4).** To a solution of **4b** (0.112 g, 0.173 mmol) in MeOH (7 mL) was added K_2CO_3 (3 mg, 0.022 mmol). After 4 h, the mixture was neutralized with DOWEX-H^+, filtered, and concentrated. FC ($CHCl_3$/MeOH 9:1) gave **4** (67 mg, 0.140 mmol, 81%) as a white solid. R_f = 0.25 ($CHCl_3$/MeOH 9:1). $[\alpha]_D$ = −36 (*c* 1.0, MeOH). IR ν_{max} cm^{-1}: 3311, 2920, 2849, 1635, 1561, 1462. ^{1}H NMR (300 MHz, DMSO-d_6): δ 1.12 (d, 3 H, *J* = 6.3 Hz), 1.23−1.32 (m, 22 H), 1.44−1.57 (m, 4 H), 2.04 (t, 2 H, *J* = 7.3 Hz), 2.46 (q, 2 H, *J* = 7.4 Hz), 3.14−3.24 (m, 4 H), 3.33−3.55 (m, 4 H), 4.53 (d, 1 H, *J* = 0 Hz), 7.78 (bs, 1 H). ^{13}C NMR (75.4 MHz, DMSO-d_6): δ 17.8, 23.7, 25.2, 27.7, 28.4, 28.6, 28.7, 28.9−30.0 (several peaks), 33.3, 35.3, 38.3, 65.2, 68.4, 70.4, 70.6, 71.9, 99.9, 172.1. HRMS: $[M + H]^+$ calcd for $C_{24}H_{47}NO_6S$, 478.3197; found, 478.3202.

(*S*-Acetyl)-*N*-(16-mercapto-palmitoyl)-2-aminoethyl-2,3,4-tri-*O*-acetyl-β-D-xylopyranoside (3b). A mixture of 2-azidoethyl-2,3,4-tri-*O*-acetyl-β-D-xylopyranoside (**3a**) (0.200 g, 0.579 mmol) and Boc_2O (0.218 g, 0.868 mmol) was dissolved in absolute EtOH (2 mL) and hydrogenated for 21 h using palladium on carbon (50 mg, 10%) under vigorous stirring and H_2 (1 atm). The suspension was filtered and concentrated, and the obtained syrup was treated with TFA (1 mL) in dry CH_2Cl_2 (5 mL) for 4 h at ambient temperature, quenched with MeOH (1 mL), and coevaporated with toluene. Crude amino sugar, **9** (0.322 g, 0.753 mmol) and DIPEA (0.111 mL, 0.637 mmol) were stirred in dry DMF (5 mL) for 5 h and coevaporated

with toluene. FC (toluene/EtOAc 1:1) gave **3b** (0.281 g, 0.445 mmol, 77%) as a white solid. R_f = 0.22 (toluene/EtOAc 1:1). $[\alpha]_D$ = −31 (*c* 1.0, $CHCl_3$). IR ν_{max} cm^{-1}: 3358, 2917, 2849, 1750, 1686, 1651, 1538, 1472, 1377, 1254, 1234. ^1H NMR (300 MHz, $CDCl_3$): δ 1.23−1.49 (m, 22 H), 1.51−1.61 (m, 4 H), 2.01 (s, 3 H), 2.02 (s, 3 H), 2.03 (s, 3 H), 2.13 (t, 2 H, *J* = 7.6 Hz), 2.29 (s, 3 H), 2.84 (t, 2 H, *J* = 7.3 Hz), 3.33 (dd, 1 H, *J* = 9.1, 11.5 Hz), 3.39−3.44 (m, 2 H), 3.60−3.68 (m, 1 H), 3.75−3.82 (m, 1 H), 4.08 (dd, 1 H, *J* = 5.2, 11.7 Hz), 4.45 (d, 1 H, *J* = 7.1 Hz), 4.89 (dd, 1 H, *J* = 7.1, 9.1 Hz), 4.95 (ddd, 1 H, *J* = 5.2, 5.2, 9.1 Hz), 5.16 (dd, 1 H, *J* = 9.1 Hz), 5.85 (bs, 1 H). ^{13}C NMR (75.4 MHz, $CDCl_3$): δ 20.8, 20.8, 20.8, 25.8, 28.9, 29.2, 29.3, 29.4−29.7 (several peaks), 30.7, 36.9, 39.2, 62.5, 69.0, 71.3, 71.7, 101.2, 169.6, 169.9, 170.1, 173.3, 196.1. HRMS: $[M + Na]^+$ calcd for $C_{31}H_{53}NO_{10}S$, 654.3282; found, 654.3284.

***N*-(16-Mercapto-palmitoyl)-2-aminoethyl-β-D-xylopyranoside (3).** To a solution of **3b** (0.159 g, 0.251 mmol) in MeOH (7 mL) was added K_2CO_3 (17 mg, 0.126 mmol). After 4 h, the mixture was neutralized with DOWEX-H^+, filtered, and concentrated. FC ($CHCl_3$/MeOH 4:1) gave **3** (0.113 g, 0.243 mmol, 97%) as a white solid. R_f = 0.54 (EtOAc/MeOH 4:1). $[\alpha]_D$ = −16 (*c* 1.0, MeOH). IR ν_{max} cm^{-1}: 3327, 2919, 2848, 1652, 1631, 1560, 1539, 1472, 1465. ^1H NMR (300 MHz, DMSO-d_6): δ 1.17−1.35 (m, 22 H), 1.44−1.57 (m, 4 H), 2.04 (t, 2 H, *J* = 7.4 Hz), 2.44 (t, 2 H, *J* = 7.3 Hz), 2.93−3.13 (m, 4 H), 3.13−3.30 (m, 3 H), 3.39−3.46 (m, 1 H), 3.63−3.71 (m, 2 H), 4.09 (d, 1 H, *J* = 7.4 Hz), 7.73 (bs, 1 H). ^{13}C NMR (75.4 MHz, DMSO-d_6): δ 23.7, 25.2, 27.7, 28.5, 28.6, 28.8, 28.9−29.0 (several peaks), 33.4, 35.3, 38.5, 65.7, 67.8, 69.5, 73.2, 76.4, 103.8, 172.2. HRMS: $[M + H]^+$ calcd for $C_{23}H_{45}NO_6S$, 464.3040; found, 464.3040.

(*S*-Acetyl)-*N*-(16-mercapto-palmitoyl)-2-aminoethyl-2,3,4,6-tetra-*O*-acetyl-β-D-glucopyranoside (2b). Peracetylated 2-azidoethyl-β-glucoside (**2a**) (0.200 g, 0.479 mmol) and Boc_2O (0.157 g, 0.719 mmol) were dissolved in absolute EtOH (3 mL) and hydrogenated for 25 h using palladium on carbon (50 mg, 10%) under vigorous stirring and H_2 (1 atm). The suspension was filtered and concentrated. The obtained syrup was treated with TFA (1 mL) in dry CH_2Cl_2 (5 mL) for 2 h at ambient temperature, quenched with MeOH (1 mL), and coevaporated with toluene. Crude amino sugar, **9** (0.266 g, 0.623 mmol) and DIPEA (0.091 mL, 0.527 mmol) were stirred in dry DMF (5 mL) for 20 h and coevaporated with toluene. FC (toluene/EtOAc 2:1 → EtOAc) gave **2b** (0.235 g, 0.334 mmol, 70%) as a white solid. R_f = 0.27 (toluene/EtOAc 2:1). $[\alpha]_D$ = −5 (*c* 1.0, $CHCl_3$). IR ν_{max} cm^{-1}: 3343, 2917, 2849, 1747, 1686, 1639, 1540, 1465, 1370, 1233. ^1H NMR (300 MHz, $CDCl_3$): δ 1.21−1.36 (m, 22 H), 1.53−1.63 (m, 4 H), 2.00 (s, 3 H), 2.02 (s, 3 H), 2.04 (s, 3 H), 2.08 (s, 3 H), 2.15 (t, 2 H, *J* = 7.6 Hz), 2.31 (s, 3 H), 2.85 (t, 2 H, *J* = 7.3 Hz), 3.40−3.47 (m, 2 H), 3.66−3.73 (m, 2 H), 3.80−3.86 (m, 1 H), 4.14 (dd, 1 H, *J* = 2.1, 12.4 Hz), 4.25 (dd, 1 H, *J* = 4.9, 12.4 Hz), 4.50 (d, 1 H, *J* = 8.0 Hz), 4.97 (dd, 1 H, *J* = 8.0, 9.3 Hz), 5.06 (dd, 1 H, *J* = 9.3, 9.6 Hz), 5.20 (dd, 1 H, *J* = 9.3, 9.6 Hz), 5.9 (bs, 1 H). ^{13}C NMR (75.4 MHz, $CDCl_3$): δ 20.7 (2 C), 20.8 (2 C), 25.8, 28.9, 29.2, 29.2, 29.5−29.7 (several peaks), 30.7, 36.8, 39.2, 61.9, 68.3, 69.5, 71.4, 72.0, 72.7, 101.0, 169.5 (2 C), 170.3, 170.7, 173.3, 196.2. HRMS: $[M + H]^+$ calcd for $C_{34}H_{57}NO_{12}S$, 704.3674; found, 704.3703.

***N*-(16-Mercapto-palmitoyl)-2-aminoethyl-β-D-glucopyranoside (2).** To a solution of **2b** (0.066 g, 0.094 mmol) in MeOH (3 mL) was added K_2CO_3 (8 mg, 0.059 mmol). After 2 h, the mixture was neutralized with DOWEX-H^+, filtered, and concentrated. FC ($CHCl_3$/MeOH 9:1) gave **2** (39 mg, 0.079 mmol, 84%) as a white solid. R_f = 0.40 ($CHCl_3$/MeOH 9:1). $[\alpha]_D$ = −7 (*c* 1.0, MeOH). IR ν_{max} cm^{-1}: 3311, 2916, 2849, 1639, 1555, 1472. ^1H NMR (300 MHz, MeOD-d_4), δ 1.30−1.42 (m, 22 H), 1.54−1.62 (m, 4 H), 2.20 (t, 2 H, *J* = 7.4 Hz), 2.50 (t, 2 H, *J* = 7.14 Hz), 3.17−3.22 (m, 1 H), 3.27−3.32 (m, 3 H), 3.33−3.39 (m, 1 H), 3.43−3.51 (m, 1 H), 3.62−3.66 (m, 1 H), 3.67−3.69 (m, 1 H), 3.85−3.95 (m, 2 H), 4.27 (d, 1 H, *J* = 7.7 Hz, H-1). ^{13}C NMR (75.4 MHz, MeOD-d_4): δ 25.0, 27.0, 29.4, 30.2, 30.3, 30.5, 30.6−30.7 (several peaks), 35.2, 37.1, 40.6, 62.7, 69.7, 71.6, 75.1, 78.0 (2 C), 104.5, 176.4. HRMS: $[M + H]^+$ calcd for $C_{24}H_{47}NO_7S$, 494.3146; found, 494.3146.

(*S*-Acetyl)-*N*-(16-mercapto-palmitoyl)-2-aminoethyl-2,2′,3,3′,4′,6,6′-hepta-*O*-acetyl-β-D-maltoside (5b). A mixture of peracetylated-2-azidoethyl-β-maltoside (**5a**) (0.400 g, 0.566 mmol) and Boc_2O (0.186 g, 0.850 mmol) was dissolved in absolute EtOH (5 mL) and hydrogenated for 18 h using palladium on carbon (50 mg, 10%) under vigorous stirring and H_2 (1 atm). The suspension was filtered and concentrated. The obtained syrup was treated with TFA (1 mL) in dry CH_2Cl_2 (5 mL) for 2 h at ambient temperature, quenched with MeOH (1 mL), and coevaporated with toluene. Crude amino sugar, **9** (0.315 g, 0.736 mmol) and DIPEA (0.108 mL, 0.623 mmol) were stirred in dry DMF (10 mL) for 1 h and coevaporated with toluene. FC (toluene/EtOAc 1:1 → EtOAc) gave **5b** (0.342 g, 0.345 mmol, 61%) as a white solid. R_f = 0.10 (toluene/EtOAc 1:1). $[\alpha]_D$ = 50 (*c* 1.0, $CHCl_3$). IR ν_{max} cm^{-1}: 3376, 2919, 2849, 1751, 1689, 1657, 1528, 1472, 1367, 1245. ^1H NMR (300 MHz, $CDCl_3$): δ 1.18−1.24 (m, 22 H), 1.50−1.65 (m, 4 H), 1.99 (s, 3 H), 2.00 (s, 3 H), 2.01 (s, 3 H), 2.02 (s, 3 H), 2.03 (s, 3 H), 2.09 (s, 3 H), 2.13 (s, 3 H), 2.15 (t, 2 H, *J* = 7.6 Hz), 2.31 (s, 3 H), 2.85 (t, 2 H, *J* = 7.3 Hz), 3.37−3.51 (m, 2 H), 3.65−3.73 (m, 2 H), 3.76−3.83 (m, 1 H), 3.93−4.00 (m, 2 H), 4.05 (dd, 1 H, *J* = 2.3, 12.4 Hz), 4.21 (dd, 1 H, *J* = 4.6, 12.4 Hz), 4.25 (dd, 1 H, *J* = 3.9, 12.4 Hz), 4.50−4.55 (m, 1 H), 4.52 (d, 1 H, *J* = 7.9 Hz), 4.81 (dd, 1 H, *J* = 7.9, 9.5 Hz), 4.85 (dd, 1 H, *J* = 4.0, 10.5 Hz), 5.05 (dd, 1 H, *J* = 9.5, 10.1 Hz), 5.24 (dd, 1 H, *J* = 8.9, 9.5 Hz), 5.35 (dd, 1 H, *J* = 9.5, 10.5 Hz), 5.40 (d, 1 H, *J* = 4.0 Hz), 5.83 (bs, 1 H). ^{13}C NMR (75.4 MHz, $CDCl_3$): δ 20.5−20.8 (7 C), 25.6, 28.7, 29.0, 29.1, 29.3, 29.4−29.5 (several peaks), 30.5, 36.5, 39.1, 61.5, 62.6, 68.0, 68.5, 69.2, 69.4, 70.0, 75.1, 76.7, 77.2, 77.6, 95.5, 100.5, 169.3, 169.6, 169.8, 170.0, 170.3, 170.4, 170.4, 173.2, 195.9. HRMS: $[M + H]^+$ calcd for $C_{46}H_{73}NO_{20}S$, 992.4519; found, 992.4536.

***N*-(16-Mercapto-palmitoyl)-2-aminoethyl-β-D-maltoside (5).** To a solution of **5b** (0.192 g, 0.194 mmol) in MeOH (10 mL) was added K_2CO_3 (13 mg, 0.097 mmol). After 3 h, the mixture was neutralized with DOWEX-H^+, filtered, and concentrated. FC ($CHCl_3$/MeOH 4:1) gave **5** (0.108 mg, 0.165 mmol, 85%) as a white solid. R_f = 0.49 (toluene/EtOH/H_2O 10:9:1). $[\alpha]_D$ = 46 (*c* 1.0, MeOH). IR ν_{max} cm^{-1}: 3329, 2920, 2848, 1621, 1554, 1469. ^1H NMR (300 MHz, DMSO-d_6): δ 1.19−1.28 (m, 22 H), 1.43−1.53 (m, 4 H), 2.04 (t, 2 H, *J* = 7.4 Hz), 2.42 (t, 2 H, *J* = 7.0 Hz), 2.99−3.09 (m, 2 H), 3.14−3.29 (m, 6 H), 3.32−3.39 (m, 1 H), 3.42−3.62 (m, 5 H), 3.67−3.74 (m, 2 H), 4.16 (d, 1 H, *J* = 8.0 Hz), 5.00 (d, 1 H, *J* = 3.6 Hz). ^{13}C NMR (75.4 MHz, DMSO-d_6): δ 24.2, 25.8, 28.2, 28.9, 29.1, 29.3, 29.4−29.5 (several peaks), 33.6, 35.9, 38.5−39.0 (1 C, overlap with solvent peak), 61.1, 61.2, 68.6, 70.2, 72.7, 73.4, 73.6, 73.8, 75.5, 76.6, 79.9, 101.2, 103.3, 173.9. HRMS: $[M + H]^+$ calcd for $C_{30}H_{57}NO_{12}S$, 656.3674; found, 656.3677.

2-Azidoethyl-2,2′,3,3′,4′-penta-*O*-benzyl-6,6′-di-*O*-tert-butyl-diphenylsilyl-β-D-maltoside (11). To a stirred solution of peracetylated 2-azidoethyl-β-maltoside **5a** (4.00 g, 5.67 mmol) in MeOH (50 mL) was added NaOMe (0.306 g, 5.67 mmol). R_f = 0.32 (toluene/EtOH/H_2O 10:9:1). After 4 h, the reaction was neutralized with DOWEX-H^+, filtered, and concentrated. Without further purification, the crude solid was dissolved in dry DMF, whereupon imidazole (6.58 g, 43.659 mmol), DMAP (3.81 g, 31.185 mmol), and TBDPSCl (6.34 mL, 24.381 mmol) were added. After 5 h, the reaction was quenched with EtOH, diluted with CH_2Cl_2, washed sequentially with 0.1 M HCl and $NaHCO_3$ (sat aq), dried, filtered, and concentrated. R_f = 0.80 (toluene/EtOH/H_2O 10:9:1). To the obtained solid and BnBr (4.05 mL, 34.02 mmol) was added NaH (1.48 g, 34.02 mmol, 55% dispersion in oil) dissolved in dry DMF (20 mL) at 0 °C under an inert atmosphere. After 5 h, additional BnBr (4.05 mL, 34.02 mmol) was added and stirred overnight. The mixture was quenched with MeOH, diluted with toluene, washed with $NaHCO_3$ (sat aq) and H_2O, dried, filtered, and concentrated. FC

(toluene → toluene/EtOAc 9:1) gave **11** (6.30 g, 4.706 mmol, 83%) as a colorless oil. R_f = 0.54 (toluene/EtOAc 19:1); $[\alpha]_D$ = 24 (*c* 1.2, $CHCl_3$). IR ν_{max} cm^{-1}: 3067, 3030, 2929, 2856, 2104, 1589, 1497, 1472, 1453, 1361, 823, 739, 700. ^1H NMR (300 MHz, $CDCl_3$): δ 1.00 (s, 9 H), 1.02 (s, 9 H), 3.39−4.04 (m, 16 H), 4.46 (d, 1 H, *J* = 7.7 Hz), 4.55−4.73 (m, 4 H), 4.77 (d, 1 H, *J* = 11.7 Hz), 4.78 (d, 1 H, *J* = 10.7 Hz), 4.87 (d, 1 H, *J* = 10.7 Hz), 4.90 (d, 1 H, *J* = 10.8 Hz), 4.95 (d, 1 H, *J* = 11.8 Hz), 4.96 (d, 1 H, *J* = 11.1 Hz), 5.74 (d, 1 H, *J* = 3.8 Hz), 7.12−7.41 (m, 37 H), 7.57−7.68 (m, 8 H). ^{13}C NMR (75.4 MHz, $CDCl_3$): δ 19.4, 19.5, 27.0, 27.0, 51.2, 62.6, 64.0, 67.9, 72.4, 72.6, 73.4, 73.6, 74.8, 75.3, 75.7, 75.8, 77.8, 80.0, 82.0, 82.3, 84.9, 96.0, 103.4, 126.9, 127.3, 127.7−127.8 (several peaks), 128.0, 128.1, 128.2, 128.4−128.5 (several peaks), 128.9, 129.6, 129.7, 129.7, 133.3, 133.4, 133.9, 133.9, 135.5, 135.7, 135.9, 136.0, 138.2, 138.6, 138.7, 138.9, 139.0. HRMS: $[M + Na]^+$ calcd for $C_{81}H_{91}N_3O_{11}Si_2$, 1360.6084; found, 1360.6369.

2-Azidoethyl-2,2′,3,3′,4′-penta-*O*-benzyl-6,6′-di-*O*-methyl-β-D-maltoside (12). To a stirred solution of **11** (2.01 g, 1.500 mmol) in dry THF (20 mL) was added TBAF (1.42 g, 4.500 mmol). After 5 h, the reaction mixture was diluted with toluene, washed with $NaHCO_3$ (sat aq) and H_2O, dried, filtered, and concentrated. R_f = 0.33 (toluene/EtOAc 1:1). To the obtained solid and MeI (0.56 mL, 9.00 mmol) dissolved in dry DMF (50 mL) was added NaH (0.262 g, 6.00 mmol, 55% dispersion in oil) at 0 °C under an inert atmosphere with stirring overnight. The reaction mixture was quenched with EtOH (10 mL), diluted with toluene, washed with $NaHCO_3$ (sat aq) and H_2O, dried, filtered, and concentrated. FC (toluene → toluene/EtOAc 1:1) gave **12** (1.146 g, 1.288 mmol, 86%) as a colorless oil. R_f = 0.48 (toluene/EtOAc 4:1). $[\alpha]_D$ = 26 (*c* 1.0, $CHCl_3$). IR ν_{max} cm^{-1}: 3063, 3031, 2885, 2104, 1497, 1453, 1359, 736, 697. ^1H NMR (300 MHz, $CDCl_3$): δ 3.34 (s, 3 H), 3.35 (s, 3 H), 3.38−3.75 (m, 12 H), 3.78 (dd, 1 H, *J* = 8.8, 9.1 Hz), 3.92 (dd, 1 H, *J* = 8.5, 9.6 Hz), 4.02−4.11 (m, 2 H), 4.45 (d, 1 H, *J* = 7.7 Hz), 4.52 (d, 1 H, *J* = 12.1 Hz), 4.60 (d, 1 H, *J* = 11.8 Hz), 4.62 (d, 1 H, *J* = 12.1 Hz), 4.62 (d, 1 H, *J* = 11.0 Hz), 4.76 (d, 1 H, *J* = 11.3 Hz), 4.82 (d, 1 H, *J* = 10.7 Hz), 4.85 (d, 1 H, *J* = 11.9 Hz), 4.90 (d, 1 H, *J* = 11.3 Hz), 4.91 (d, 1 H, *J* = 10.7 Hz), 4.96 (d, 1 H, *J* = 11.9 Hz), 5.66 (d, 1 H, *J* = 3.6 Hz), 7.14−7.20 (m, 5 H), 7.22−7.32 (m, 20 H). ^{13}C NMR (75.4 MHz, $CDCl_3$): δ 51.2, 59.3, 59.3, 68.1, 70.9, 71.0, 71.3, 72.1, 73.4, 74.1, 74.4, 74.8, 75.2, 75.6, 77.7, 79.4, 82.1, 82.3, 84.9, 97.0, 103.7, 126.7, 127.2, 127.6, 127.7, 127.8, 127.8, 127.9, 127.9, 128.0, 128.3, 128.4−128.4 (several peaks), 128.5, 138.1, 138.4, 138.7, 138.9, 138.9. HRMS: $[M + Na]^+$ calcd for $C_{51}H_{59}N_3O_{11}$, 912.4042; found, 912.4046.

(*S*-Acetyl)-*N*-(16-mercapto-palmitoyl)-2-aminoethyl-6,6′-di-*O*-methyl-β-D-maltoside (13). Compound **12** (0.163 g, 0.183 mmol) was dissolved in EtOH/HOAc (5 mL, 9:1) and hydrogenated for 23 h using palladium hydroxide on carbon (70 mg, 20%) under vigorous stirring and H_2 (1 atm). The suspension was filtered and concentrated. Crude amino sugar, **9** (0.102 g, 0.239 mmol) and DIPEA (0.035 mL, 0.201 mmol) were stirred in dry DMF (3 mL) for 4 h and coevaporated with toluene. FC (EtOAc/MeOH/CH_2Cl_2/H_2O 20:2:2:1) gave **13** (87 mg, 0.120 mmol, 65%) as a white solid. R_f = 0.23 (EtOAc/MeOH/H_2O 20:2:1). $[\alpha]_D$ = 30 (*c* 1.1, $CHCl_3$). IR ν_{max} cm^{-1}: 2917, 2849, 1696, 1646, 1545, 1465, 1215. ^1H NMR (300 MHz, $CDCl_3$): δ 1.18−1.35 (m, 22 H), 1.49−1.59 (m, 4 H), 2.16 (t, 2 H, *J* = 7.0 Hz), 2.30 (s, 3 H), 2.84 (t, 2 H, *J* = 7.3 Hz), 3.35 (s, 3 H), 3.36 (s, 3 H), 3.29−3.88 (m, 16 H), 4.30 (d, 1 H, *J* = 7.7 Hz), 5.07 (d, 1 H, *J* = 3.1 Hz), 7.12 (bs, 1 H). ^{13}C NMR (75.4 MHz, $CDCl_3$): δ 25.5, 25.9, 29.0, 29.3, 29.6−29.9 (several peaks), 30.7, 36.5, 39.6, 59.1, 59.3, 69.4, 70.0, 71.4, 72.0 (2 C), 72.5, 73.0, 73.7, 74.0, 76.1, 80.5, 101.8, 102.9, 174.8, 196.2. HRMS: $[M + H]^+$ calcd for $C_{34}H_{63}NO_{13}S$, 726.4093; found, 726.4093.

***N*-(16-Mercapto-palmitoyl)-2-aminoethyl-6,6′-di-*O*-methyl-β-D-maltoside (6).** To a solution of **13** (47 mg, 0.065 mmol) in MeOH (3 mL) was added K_2CO_3 (7 mg, 0.051 mmol). After 1 h, the mixture was neutralized with DOWEX-H^+, filtered, and concentrated. FC (EtOAc/CH_2Cl_2/MeOH/H_2O 20:2:2:1) gave **6** (37 mg, 0.054 mmol, 83%) as a white solid. R_f = 0.16 (EtOAc/MeOH/H_2O 20:2:1). $[\alpha]_D$ = 44 (*c* 0.8, MeOH). IR ν_{max} cm^{-1}: 2919, 2849, 1643, 1551, 1468. ^1H NMR (300 MHz, MeOD-d_4): δ 1.29−1.42 (m, 22 H), 1.54−1.62 (m, 4 H), 2.20 (t, 2 H, *J* = 7.6 Hz), 2.49 (t, 2 H, *J* = 7.1 Hz), 3.22−3.27 (m, 2 H), 3.34−3.39 (m, 1 H), 3.38 (s, 3 H), 3.39 (s, 3 H), 3.42−3.72 (m, 11 H), 3.75−3.81 (m, 1 H), 3.84−3.91 (m, 1 H), 4.29 (d, 1 H, *J* = 7.7 Hz), 5.10 (d, 1 H, *J* = 3.6 Hz). ^{13}C NMR (75.4 MHz, MeOD-d_4): δ 25.0, 27.0, 29.4, 30.2, 30.3, 30.4, 30.6−30.7, 35.2, 37.1, 40.5, 59.3, 59.5, 69.8, 71.5, 72.4, 73.4, 73.5, 74.1, 74.5, 75.0, 75.3, 77.5, 81.8, 103.1, 104.4, 176.5. HRMS: $[M + H]^+$ calcd for $C_{32}H_{61}NO_{12}S$, 684.3987; found, 684.3989.

2-Azidoethyl-2,2′,2″,3,3′,3″,4″,6,6′,6″-undeca-*O*-acetyl-β-D-maltotrioside (7a). A solution of maltotriose (5.00 g, 9.91 mmol), NaOAc (0.10 g, 1.22 mmol), and Ac_2O (10 mL, 10.80 g, 0.105 mol) in toluene (25 mL) was heated to reflux. After 2 h, H_2O was added, and the solution was neutralized with 1 M NaOH(aq), dried, filtered, and concentrated. Crude peracetylated maltotriose, 2-azidoethanol (3.45 g, 39.64 mmol), and 4 Å MS were stirred in dry $CHCl_2$ (20 mL), whereupon $BF_3 \cdot OEt_2$ (3.73 mL, 4.22 g, 29.74 mmol) was added and stirred overnight. The mixture was filtered through Celite 545, diluted with CH_2Cl_2, washed sequentially $NaHCO_3$(s) and H_2O, dried, filtered, and concentrated. FC (petroleum ether (60−80)/EtOAc 1:1 → 1:2) gave **7a** (4.38 g, 4.01 mmol, 44%) as a colorless solid. R_f = 0.62 (petroleum ether (60−80 °C)/EtOAc 1:2). $[\alpha]_D$ = 73 (*c* 1.0, $CHCl_3$). IR ν_{max} cm^{-1}: 2964, 2109, 1751, 1373, 1237. ^1H NMR (300 MHz, $CDCl_3$): δ 1.98 (s, 3 H), 1.99 (s, 3 H), 2.00 (s, 3 H), 2.01 (s, 3 H), 2.01 (s, 3 H), 2.02 (s, 3 H), 2.05 (s, 3 H), 2.09 (s, 3 H), 2.15 (s, 3 H), 2.17 (s, 3 H), 3.26 (ddd, 1 H, *J* = 3.4, 4.9, 13.4 Hz), 3.47 (ddd, 1 H, *J* = 3.4, 8.2, 13.4 Hz), 3.66−3.75 (m, 2 H), 3.89−4.00 (m, 5 H), 4.02 (dd, 1 H, *J* = 2.3, 12.4 Hz), 4.16−4.26 (m, 2 H), 4.29 (dd, 1 H, *J* = 4.2, 12.1 Hz), 4.45 (dd, 1 H, *J* = 2.2, 12.3 Hz), 4.51 (dd, 1 H, *J* = 3.0, 12.2 Hz), 4.61 (d, 1 H, *J* = 7.8 Hz), 4.73 (dd, 1 H, *J* = 4.1, 10.3 Hz), 4.81−4.87 (m, 2 H), 5.06 (dd, 1 H, *J* = 9.6, 10.1 Hz), 5.23−5.32 (m, 2 H), 5.35−5.42 (m, 3 H). ^{13}C NMR (75.4 MHz, $CDCl_3$): δ 20.4−20.7 (10 C), 50.3, 61.3, 62.3, 62.7, 67.8, 68.4, 68.5, 68.8, 69.2, 69.3, 70.3, 71.6, 71.8, 72.1, 72.5, 73.6, 75.1, 95.5, 95.6, 100.0, 169.2, 169.5, 169.5, 169.6, 169.9, 170.2, 170.3, 170.3, 170.4, 170.3. HRMS: $[M + Na]^+$ calcd. for $C_{40}H_{55}N_3O_{26}$, 1016.2966; found, 1016.2972.

(*S*-Acetyl)-*N*-(16-mercapto-palmitoyl)-2-aminoethyl-2,2′,2″,3,3′,3″,4″,6,6′,6″-undeca-*O*-acetyl-β-D-maltotrioside (7b). Compound **7a** (0.400 g, 0.402 mmol) and Boc_2O (0.131 g, 0.603 mmol) were dissolved in absolute EtOH (5 mL, 99.5%) and hydrogenated for 19 h using palladium on carbon (50 mg, 10%) under vigorous stirring and H_2 (1 atm). The obtained syrup was treated with TFA (1 mL) in dry CH_2Cl_2 (5 mL) for 3 h at room temperature, quenched with EtOH (1 mL), and coevaporated with toluene. Crude amino sugar, **9** (0.223 g, 0.523 mmol) and DIPEA (0.077 mL, 0.442 mmol) were stirred in dry DMF (10 mL) for 6 h and coevaporated with toluene. FC (toluene/EtOAc 1:1 → EtOAc) gave **7b** (0.351 g, 0.274 mmol, 68%) as a white solid. R_f = 0.21 (toluene/EtOAc 1:1). $[\alpha]_D$ = 73 (*c* 1.0, $CHCl_3$). IR ν_{max} cm^{-1}: 3411, 2926, 2854, 1755, 1691, 1534, 1369, 1237. ^1H NMR (300 MHz, $CDCl_3$): δ 1.25−1.38 (m, 22 H), 1.54−1.61 (m, 4 H), 1.99 (s, 3 H), 2.00 (s, 3 H), 2.00 (s, 3 H), 2.02 (s, 3 H), 2.02 (s, 3 H), 2.03 (s, 3 H), 2.05 (s, 3 H), 2.10 (s, 3 H), 2.15 (s, 3 H), 2.17 (s, 3 H), 2.14−2.19 (m, 2 H), 2.32 (s, 3 H), 2.86 (t, 2 H, *J* = 7.3 Hz), 3.42−3.51 (m, 2 H), 3.71−3.83 (m, 3 H), 3.91−3.98 (m, 4 H), 4.06 (dd, 1 H, *J* = 2.0, 12.5 Hz), 4.16−4.32 (m, 3 H), 4.46−4.56 (m, 3 H), 4.74 (dd, 1 H, *J* = 4.1, 10.4 Hz), 4.80 (dd, 1 H, *J* = 8.0, 9.3 Hz), 4.86 (dd, 1 H, *J* = 4.0, 10.4 Hz), 5.07 (dd, 1 H, *J* = 9.8, 9.9 Hz), 5.23−5.33 (m, 2 H), 5.36−5.42 (m, 3 H), 5.86 (bs, 1 H). ^{13}C NMR (75.4 MHz, $CDCl_3$): δ 20.5−20.8 (10 C), 25.7, 28.8, 29.1, 29.1, 29.4−29.6 (several peaks), 30.6, 36.6, 39.2, 61.4, 62.3, 62.7, 68.0, 68.5, 69.0, 69.3, 69.5, 70.1, 70.4, 71.7, 72.2, 72.4, 72.5, 73.6, 75.1, 95.6, 95.8, 100.5, 169.4, 169.6, 169.7, 169.8, 170.0, 170.3, 170.4, 170.4, 170.5, 170.6, 173.2,

195.9. HRMS: $[M + H]^+$ calcd for $C_{58}H_{89}NO_{28}S$, 1280.5365; found, 1280.5373.

***N*-(16-Mercapto-palmitoyl)-2-aminoethyl-β-D-maltotrioside (7).** To a solution of **7b** (0.368 g, 0.287 mmol) in MeOH (10 mL) was added K_2CO_3 (55 mg, 0.395 mmol). After 3 h, the mixture was neutralized with DOWEX-H^+, filtered, and concentrated. FC ($CHCl_3$/MeOH 4:1 → $CHCl_3$/MeOH 3:2) gave **7** (0.172 mg, 0.210 mmol, 73%) as a white solid. R_f = 0.43 (toluene/EtOH/H_2O 10:9:1). $[\alpha]_D$ = 73 (*c* 1.0, $CHCl_3$). IR ν_{max} cm^{-1}: 2917, 2849, 1645, 1553, 1467, 1368. ^1H NMR (300 MHz, DMSO-d_6): δ 1.20−1.30 (m, 22 H), 1.43−1.52 (m, 4 H), 2.05 (t, 2 H, *J* = 7.4 H), 2.43 (t, 2 H, *J* = 7.0 Hz), 2.99−3.08 (m, 2 H), 3.12−3.84 (m, 20 H), 4.17 (d, 1 H, *J* = 7.97 Hz), 4.98 (d, 1 H, *J* = 3.9 Hz), 5.00 (d, 1 H, *J* = 4.2 Hz). ^{13}C NMR (75.4 MHz, DMSO-d_6): δ 23.9, 25.5, 28.0, 28.7, 28.9−29.1 (several peaks), 33.6, 35.6, 38.5−39.0 (1 C, overlap with solvent peak), 60.4, 60.8, 61.0, 68.4, 70.0, 72.0, 72.1, 72.6, 73.1, 73.3, 73.4, 73.7, 75.3, 76.3, 79.7, 80.0, 100.8, 101.0, 103.1, 173.1. HRMS: $[M + H]^+$ calcd for $C_{36}H_{67}NO_{17}S$, 818.4203; found, 818.4208.

■ ASSOCIATED CONTENT

Supporting Information. Ellipsometric, contact angle, and IRAS data for the mixed SAMs. This material is available free of charge via the Internet at http://pubs.acs.org.

■ AUTHOR INFORMATION

Corresponding Author
*e-mail: ted@ifm.liu.se.

■ ACKNOWLEDGMENT

The authors acknowledge support from the AMBIO project (NMP-CT-2005-011827) funded by the European Commission's Sixth Framework Programme. The views expressed in this publication reflect only those of the authors, and the Commission is not liable for any use that may be made of the information contained herein.

■ REFERENCES

(1) Varki, A.; Cummings, R.; Esko, J.; Freeze, H.; Hart, G.; Marth, J. *Essentials of Glycobiology*; Cold Spring Harbor Laboratory Press: New York, 1999.
(2) Varma, A. J.; Kennedy, J. F.; Galgali, P. *Carbohydr. Polym.* **2004**, *56*, 429–445.
(3) Finkenstadt, V. L. *Appl. Microbiol. Biotechnol.* **2005**, *67*, 735–745.
(4) Dai, L.; StJohn, H. A. W.; Bi, J.; Zientek, P.; Chatelier, R. C.; Griesser, H. J. *Surf. Interface Anal.* **2000**, *29*, 46–55.
(5) Liu, Y.; Chan-Park, M. B. *Biomaterials* **2009**, *30*, 196–207.
(6) Löfås, S.; Johnsson, B. *J. Chem. Soc., Chem. Commun.* **1990**, 1526–1528.
(7) Fukui, S.; Feizi, T.; Galustian, C.; Lawson, A. M.; Chai, W. *Nat. Biotechnol.* **2002**, *20*, 1011–1017.
(8) Morra, M.; Cassineli, C. *J. Biomater. Sci., Polym. Ed.* **1999**, *10*, 1107–1124.
(9) Martwiset, S.; Koh, A. E.; Chen, W. *Langmuir* **2006**, *22*, 8192–8196.
(10) Cao, X.; Pettit, M. E.; Conlan, S. L.; Wagner, W.; Ho, A. D.; Clare, A. S.; Callow, J. A.; Callow, M. E.; Grunze, M.; Rosenhahn, A. *Biomacromolecules* **2009**, *10*, 907–915.
(11) Prime, K. L.; Whitesides, G. M. *Science* **1991**, *252*, 1164–1167.
(12) Hederos, M.; Konradsson, P.; Liedberg, B. *Langmuir* **2005**, *21*, 2971–2980.
(13) Ederth, T.; Ekblad, T.; Pettitt, M. E.; Conlan, S. L.; Du, C.-X.; Callow, M. E.; Callow, J. A.; Mutton, R.; Clare, A. S.; D'Souza, F.; Donnelly, G.; Bruin, A.; Willemsen, P.; Su, X. J.; Wang, S.; Zhao, Q.; Hederos, M.; Konradsson, P.; Liedberg, B. *ACS Appl. Mater. Interfaces* **2011**, *3*, 3890–3901.
(14) Luk, Y.-Y.; Kato, M.; Mrksich, M. *Langmuir* **2000**, *16*, 9604–9608.
(15) Metzke, M.; Guan, Z. *Biomacromolecules* **2007**, *9*, 208–215.
(16) Bandyopadhyay, D.; Prashar, D.; Luk, Y.-Y. *Langmuir* **2011**, *27*, 6124–6131.
(17) Pale-Grosdemange, C.; Simon, E. S.; Prime, K. L.; Whitesides, G. M. *J. Am. Chem. Soc.* **1991**, *113*, 12–20.
(18) Wang, R. L. C.; Kreuzer, H. J.; Grunze, M. *J. Phys. Chem. B* **1997**, *101*, 9767–9773.
(19) Harder, P.; Grunze, M.; Dahint, R.; Whitesides, G. M.; Laibinis, P. E. *J. Phys. Chem. B* **1998**, *102*, 426–436.
(20) Chapman, R. G.; Ostuni, E.; Takayama, S.; Holmlin, R. E.; Yan, L.; Whitesides, G. M. *J. Am. Chem. Soc.* **2000**, *122*, 8303–8304.
(21) Railkin, A. I. *Marine Biofouling: Colonization Processes and Defenses*. CRC Press: Boca Raton, FL, 2003.
(22) Borgh, A.; Ekeroth, J.; Petoral, R. M., Jr.; Uvdal, K.; Konradsson, P.; Liedberg, B. *J. Colloid Interface Sci.* **2006**, *295*, 41–49.
(23) Svedhem, S.; Öhberg, L.; Borrelli, S.; Valiokas, R.; Andersson, M.; Oscarson, S.; Svensson, S. C. T.; Liedberg, B.; Konradsson, P. *Langmuir* **2002**, *18*, 2848–2858.
(24) Grant, C. F.; Kanda, V.; Yu, H.; Bundle, D. R.; McDermott, M. T. *Langmuir* **2008**, *24*, 14125–14132.
(25) Chernyak, A. Y.; Sharma, G. V. M.; Kononov, L. O.; Krishna, P. R.; Levinsky, A. B.; Kochetkov, N. K.; Rama Rao, A. V. *Carbohydr. Res.* **1992**, *223*, 303–309.
(26) Hadfield, A. F.; Lazo, J. S.; Sartorelli, A. C. *Carbohydr. Res.* **1979**, *77*, 51–59.
(27) Mikata, Y.; Kakuchi, K.; Yano, S. Fullerene derivative and composition comprising the same. Jap. pat. JP2002-212197A, July 31, 2002.
(28) Ohlsson, J.; Magnusson, G. *Tetrahedron* **2000**, *56*, 9975–9984.
(29) Porter, M. D.; Bright, T. B.; Allara, D. L.; Chidsey, C. E. D. *J. Am. Chem. Soc.* **1987**, *109*, 3559–3568.
(30) Nuzzo, R. G.; Dubois, L. H.; Allara, D. L. *J. Am. Chem. Soc.* **1990**, *112*, 558–569.
(31) Malysheva, L.; Onipko, A.; Valiokas, R.; Liedberg, B. *J. Phys. Chem. B* **2005**, *109*, 13221–13227.
(32) Valiokas, R.; Svedhem, S.; Östblom, M.; Svensson, S. C. T.; Liedberg, B. *J. Phys. Chem. B* **2001**, *105*, 5459–5469.
(33) Clegg, R. S.; Hutchison, J. E. *Langmuir* **1996**, *12*, 5239–5243.
(34) Tam-Chang, S.-W.; Biebuyck, H. A.; Whitesides, G. M.; Jeon, N.; Nuzzo, R. G. *Langmuir* **1995**, *11*, 4371–4382.
(35) Jenny, N. S.; Mann, K. G. In *Thrombosis and Hemorrhage*; Loscalzo, J., Schafer, A. I., Eds.; Lippincott Williams & Wilkins: Philadelphia, 2003; pp 1−21.
(36) Lee, R. G.; Adamson, C.; Kim, S. W. *Thromb. Res.* **1974**, *4*, 485–490.
(37) Kidoaki, S.; Matsuda, T. *Langmuir* **1999**, *15*, 7639–7646.
(38) Benesch, J.; Svedhem, S.; Svensson, S. C. T.; Valiokas, R.; Liedberg, B.; Tengvall, P. *J. Biomater. Sci., Polym. Ed.* **2001**, *12*, 581–597.
(39) Schilp, S.; Rosenhahn, A.; Pettitt, M. E.; Bowen, J.; Callow, M. E.; Callow, J. A.; Grunze, M. *Langmuir* **2009**, *25*, 10077–10082.
(40) Prime, K. L.; Whitesides, G. M. *J. Am. Chem. Soc.* **1993**, *115*, 10714–10721.
(41) Sokal, R. R.; Rohlf, F. J. *Biometry*, 4th ed.; W. H. Freeman: New York, 2005.
(42) Callow, M. E.; Callow, J. A.; Ista, L. K.; Coleman, S. E.; Nolasco, A. C.; Lopez, G. P. *Appl. Environ. Microbiol.* **2000**, *66*, 3249–3254.
(43) Bennett, S. M.; Finlay, J. A.; Gunari, N.; Wells, D. D.; Meyer, A. E.; Walker, G. C.; Callow, M. E.; Callow, J. A.; Bright, F. V.; Detty, M. R. *Biofouling* **2010**, *26*, 235–246.
(44) Schilp, S.; Kueller, A.; Rosenhahn, A.; Grunze, M.; Pettitt, M. E.; Callow, M. E.; Callow, J. A. *Biointerphases* **2007**, *2*, 143–150.
(45) Aldred, N.; Li, G.; Gao, Y.; Clare, A. S.; Jiang, S. *Biofouling* **2010**, *26*, 673–683.

(46) Callow, M. E.; Callow, J. A.; Pickett-Heaps, J. D.; Wetherbee, R. *J. Phycol.* **1997**, *33*, 938–947.
(47) Finlay, J. A.; Callow, M. E.; Schultz, M. P.; Swain, G. W.; Callow, J. A. *Biofouling* **2002**, *18*, 251–256.
(48) Callow, M. E.; Jennings, A. R.; Brennan, A. B.; Seegert, C. E.; Gibson, A.; Wilson, L.; Feinberg, A.; Baney, R.; Callow, J. A. *Biofouling* **2002**, *18*, 237–245.
(49) Gottlieb, H. E.; Kotlyar, V.; Nudelman, A. *J. Org. Chem.* **1997**, *62*, 7512–7515.

■ NOTE ADDED AFTER ASAP PUBLICATION

This article was published ASAP on November 23, 2011. The headings of paragraphs 24 and 25 of the Experimental Section have been modified. The correct version was published on December 13, 2011.